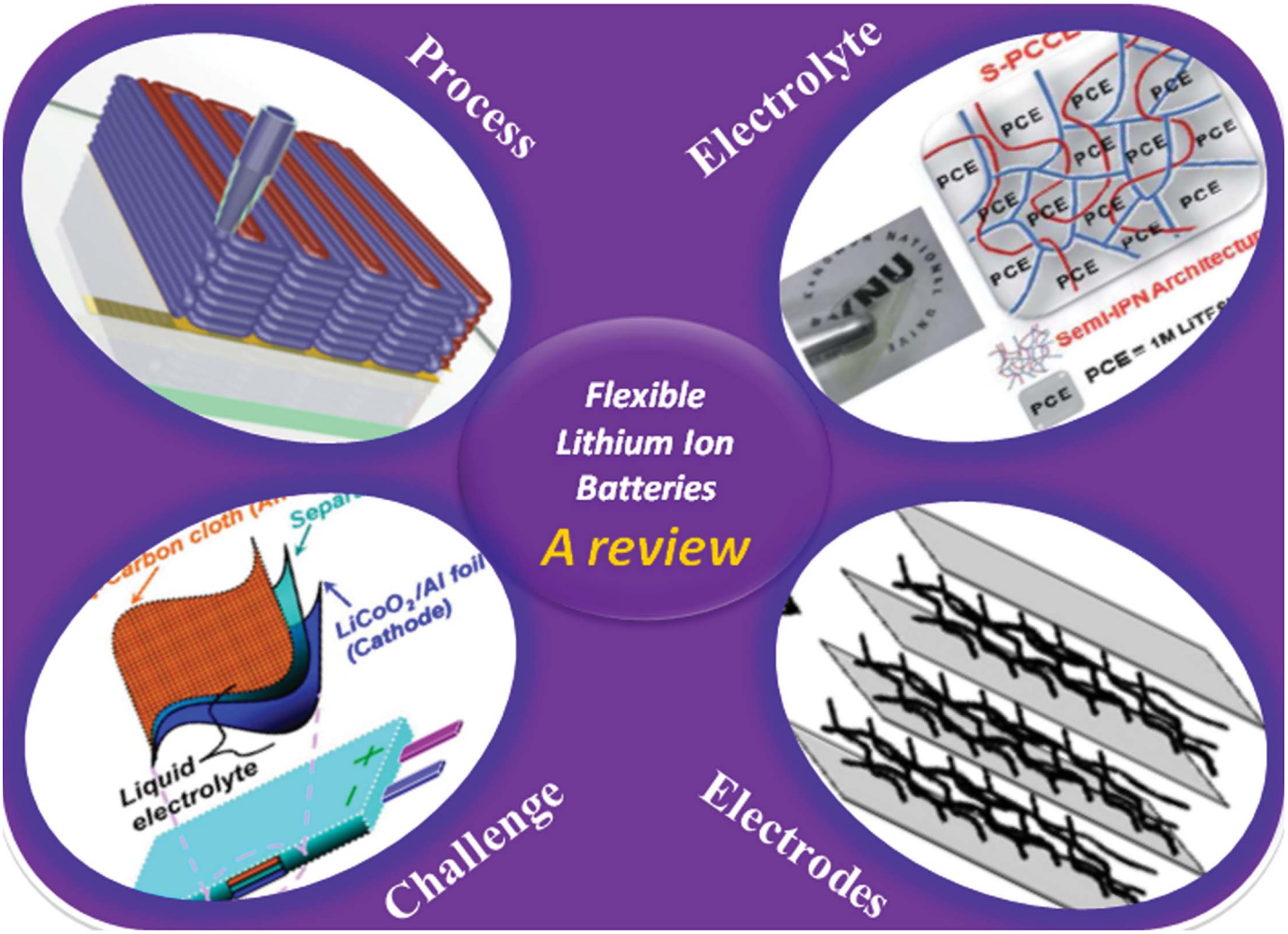

Showcasing the review of flexible lithium ion batteries presented by Prof. Xueliang (Andy) Sun, Department of Mechanical and Materials Engineering, The University of Western University.

Title: Flexible Rechargeable Lithium Ion Batteries: Advances and Challenges in Materials and Process Technologies

A comprehensive review of flexible lithium ion batteries is presented. The review proceeds in terms of the processes for making electrodes and full LIB cells so as to emphasize the materials and process technologies. The development of solid state electrolytes, the fundamental understanding and simulation of flexible LIBs are also addressed. The review concludes with an emphasis on the potential application of printing processes in flexible LIB fabrication.

As featured in:

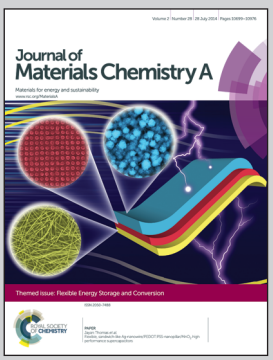

See Yuhai Hu and Xueliang Sun, *J. Mater. Chem. A*, 2014, **2**, 10712.

ROYAL SOCIETY OF CHEMISTRY

www.rsc.org/MaterialsA

Registered charity number: 207890

Journal of Materials Chemistry A

FEATURE ARTICLE

View Article Online
View Journal | View Issue

Cite this: *J. Mater. Chem. A*, 2014, **2**, 10712

Flexible rechargeable lithium ion batteries: advances and challenges in materials and process technologies

Yuhai Hu and Xueliang Sun*

Received 11th February 2014
Accepted 23rd April 2014

DOI: 10.1039/c4ta00716f

www.rsc.org/MaterialsA

Flexible batteries possess several unique features including high flexibility, lightweight and easy portability, high specific power and energy density, and remarkable rate capability, *etc.* So far, many different kinds of flexible batteries have been invented. The batteries, according to the electrochemical processes in a cell, can be categorized as flexible alkaline batteries, plastic batteries (or all-polymer batteries), polymer lithium-metal batteries (with lithium foil as an anode), and flexible rechargeable lithium ion batteries (LIBs), *etc.* Among these, flexible LIBs attract more rapidly increasing attention. As compared to the conventional rechargeable LIBs, fabrication of flexible LIBs is more challenging. An optimal match among the core components, *i.e.*, nanostructured electrode materials, shape-conformable solid electrolytes, and soft current collectors should be achieved, so that the batteries maintain stable electrochemical performances even though they are deformed to fit the powered devices. Thus, fabrication of such batteries is not cost-effective and hence, is also inefficient. In the search for the potential core components for flexible LIBs, much progress has been made in screening solid state electrolytes, soft current collectors and electrode materials, and in electrode design and full LIB cell assembly (particularly

Department of Mechanical and Materials Engineering, Faculty of Engineering, The University of Western Ontario, London, Ontario, N6A 5B7, Canada. E-mail: xsun9@uwo.ca; Fax: +519-6613020; Tel: +519-6612111 ext. 87759

Yuhai Hu is currently a PhD candidate in Prof. Xueliang (Andy) Sun's Nanomaterials and Energy Group at Western University, Canada. Mr Hu received his BSc in Chemistry at Shenyang Normal University, China, in 1996. He got his Ph D in Chemistry at Nanjing University in 2001. His research focused on developing novel catalysts for catalytic reduction of NOx by CO. He had worked for several years in Japan and Canada before joining Prof. Sun's group in 2011. His current research interest is to synthesize and characterize nanomaterials used as anode materials for lithium ion batteries.

Xueliang (Andy) Sun is a Full Professor and a Canada Research Chair at the University of Western Ontario, Canada. Dr Sun received his PhD in Materials Chemistry under direction of Prof. George Thompson in 1999 at the University of Manchester, UK, followed by work as a postdoctoral fellow under direction of Prof. Keith Mitchell at the University of British Columbia, Canada, and as a Research Associate under direction of Prof. Jean-Pol Dodelet at l'Institut National de la Recherche Scientifique (INRS), Canada. His current research interests are associated with synthesis of low-dimensional nanomaterials for electrochemical energy storage and conversion. His research focus is on design and synthesis of various one-dimensional nanostructures such as nanotubes, nanowires, nanoparticles and nanofilms as well as their composites as electrocatalysis and catalyst support in fuel cells and as anode and cathodes in lithium ion batteries and metal–air batteries. His website: http://www.eng.uwo.ca/people/asun/publications.htm.

in managing to get the three core components to work harmonically). There are also studies focusing on fundamental understanding and simulation of fully flexible LIBs. They reliably anticipate and describe the battery performances that are not easily explored experimentally using the present state-of-the-art technologies. In this review, we systematically summarize the advances in flexible LIBs research, with focus on the development of flexible electrodes. The review proceeds in terms of the processes for making electrodes and full LIB cells so as to emphasize the materials and process technologies. The development of solid state electrolytes and the fundamental understanding and simulation of flexible LIBs are also addressed. The review concludes with a perspective according to the author's experience in the related field, and the potential application of printing processes in flexible LIB fabrication is especially emphasized.

1. Introduction

The unique features that make flexible batteries a greatly attractive powering system include high flexibility, high specific power and energy density, remarkable rate capability, lightweight, and ease of portability, *etc.* The rapid development of soft portable electronic devices, such as rollup displays, wearable devices, radio-frequency identification tags, and integrated circuit smart cards, *etc.*, has stimulated the research and development of flexible batteries that are able to be embedded into these devices and power them.[1,2] So far, many different types of flexible batteries have been invented, including flexible alkaline batteries, plastic batteries (or all-polymer batteries), polymer lithium-metal batteries, and flexible rechargeable lithium ion batteries (LIBs), *etc.* Generally, irrespective of the composites and hence the principle of a flexible battery, optimal match among the electrode materials, electrolytes, and soft and mechanically strong current collectors should be achieved. Thus, the batteries can maintain high capacity, high rate capability and cycling stability, good conductivity and robust flexibility. It has been one of the biggest challenges to optimize match among the electrode materials, electrolytes, and soft and current collectors in flexible batteries research and development.

Flexible batteries have a history of almost 100 years. Earlier studies focused on flexible alkaline batteries[3–6] and all-polymer batteries (or plastic batteries).[7–11] Later, polymer lithium-metal batteries began to gain more interest.[12–15] Recent research interest is being intensively concentrated on flexible LIBs.[16–18] Compared to other types of batteries, flexible LIBs possess higher energy density, higher output voltage, longer life and environmentally benign operation, *etc.*[19] Flexible LIBs share the same principles of "conventional" LIBs, which have been described in many papers.[18,19] So far, not only has great progress been made in the development of the core battery composites: electrode materials, shape-conformable solid electrolytes, and soft and mechanically strong current collectors, significant advances have also been achieved in the battery design. Many novel technologies and processes have been invented to make flexible electrodes and to fabricate full batteries with high performance. The materials development has been considerably spurred by the advances in nanoscience and nanotechnology, which offer many different kinds of novel one-dimensional (1D) and two-dimensional (2D) nanosized materials such as nanostructured carbon (nanotubes, carbon fibers, and graphene), nanostructured silicon (nanoparticles (NPs) and nanowires (NWs)), nanostructured metal oxides, and nanostructured conventional cathode materials, *etc.*[20–34] The invention/introduction of conventional or new technologies and processes such as self-assembly, sputtering, deposition, painting, and printing, in turn, brings advances in the electrode materials research and development.[35–40] Nevertheless, the challenges for flexible LIBs research are still huge.

(1) Current batteries are unable to sustain stable power and energy supply and cyclic stability for uses under frequent mechanical strains, such as bending, twisting or other deformations. This mostly results from the facts: (a) the flexibility and strength of the electrodes is not high enough because intrinsically inflexible materials are used; (b) the contact among battery constituent materials is poor, particularly the active materials–substrate contact; (c) operation at deformed states leads to severe degradation of the electrochemical and mechanical properties; and (d) electrolyte leakage happens under certain circumstances, and thus,

(2) the development of mechanically strong flexible electrodes is required. This may be achieved by growing/embedding active electrode materials on fully flexible conductive substrates without the use of conductive additives or binders.

(3) Flexible polymer solid electrolytes with optimal mechanical properties and ionic conductivity still need to be developed.

(4) Optimization of battery production and packaging in order to increase productivity and reduce cost, for which advanced process technologies should be introduced and adopted.

In this review, we will systematically summarize the advances in flexible LIBs research, with an emphasis on the development of flexible electrodes. It is important to notice that the design of materials and electrodes is highly dependent on (and to some extent, is determined by) a workable fabrication process. Therefore, this review proceeds in terms of the processes for making electrodes and for full LIB cells assembly as well as the electrolyte selection. The review also briefly summarizes the development of the shape-conformable solid electrolytes. Fundamental understanding and simulation of the performances of fully flexible batteries is also addressed as they reliably anticipate and describe the battery performances that are not easily explored experimentally using the present state-of-the-art technologies. The review concludes with a detailed perspective according to the author's experience in the related field, and the potential application of printing process is specially discussed.

It is worth mentioning that in the literature, flexible batteries are also expressed as stretchable batteries,[41,42] foldable/bendable batteries,[43,44] cable batteries,[17,45] and plastic batteries,[46–50] *etc.* In this review, all the related studies are addressed as "flexible" batteries. Moreover, there are a huge number of papers in this field, which involve many different kinds of systems (*e.g.*, electrode materials, electrolyte, and packaging, *etc.*); hence, it is impossible for us to list all of them. Instead, for each sub-topic, we select several representative papers that effectively demonstrate the materials and the state-of-the-art process technologies, particularly concerning the full cell assembly and electrochemical property evaluation. These papers are presented with an emphasis on critically analyzing electrode materials, electrode preparation, electrolyte selection, cell assembly (particularly full cell packaging), electrochemical performance, and the advantage and disadvantage, so that this review can be as beneficial as possible to the readers. The review is kept neutral, but for some important works, the advantages and issues in practical application of the electrode and full cell configuration are discussed.

2. Flexible electrodes

Flexible rechargeable LIBs share the same core battery components and working principle with the conventional LIBs. However, as with the flexible LIBs, both anode and cathode materials must be combined with a suitable medium to achieve high flexibility and mechanical strength. For example, for a workable flexible electrode, the active materials should remain integrated with underlying current collector when a battery is folded, bent or even twisted. The configuration of flexible electrodes, to some extent, determines a full battery design. Usually, two approaches are used for designing flexible electrodes. The first one is to cast (or deposit) active materials on a flexible substrate embedded with a current collector (Type-I). The other method involves blending active materials with a second electrochemically stable, electrically conductive, and mechanically strong composite (usually 1D or 2D nanostructured carbon) to achieve freestanding electrode (Type-II). Flexible substrate as a backing composite is not needed in this type of electrode. These two approaches possess their own advantages and disadvantages. For the Type-I electrodes, the presence of a flexible substrate, *e.g.*, polymer films, offers mechanical strength for the electrode. However, binder (usually electrically non-conductive) is required to hold the active materials on the substrate. The use of an electrically non-conductive binder combined with the substrate that usually has no contribution to lithium storage but accounts for some weight of the electrode, decreases the overall energy density of the full battery.[18,51,52] Furthermore, the substrate usually has limited surface area and thus, there is a limitation for the active materials–current collector contact. Consequently, the active materials are easily detached from the electrode when the battery is deformed. The majority of the Type-II electrodes are currently being investigated at the laboratorial scale, due to their limited mechanical strength, although they possess relatively higher energy density as a result of their lack of binder and substrate. Low efficiency of fabricating such electrodes is another issue that limits their practical application.

In this part, the research and development of the two types of flexible electrodes will be reviewed in detail. To best demonstrate the entire scope, the Type-I flexible electrodes are categorized as flexible cathodes and flexible anodes, which, on the base of the used substrate, are further categorized as flexible electrodes on conductive substrates and non-conductive substrates. The Type-II electrodes are categorized as flexible cathodes and flexible anodes, and the flexible anodes are further categorized as carbon in 2D and 3D assemblies and assembly of carbon and high-capacity nanomaterials.

2.1 Flexible substrate supported electrodes (Type-I)

For this type of flexible electrodes, flexibility and mechanical strength are dependent on the substrate used. The substrate can be electrically conductive (also works as a current collector) or non-conductive. The conductive substrates include metal foil and carbon-based films and membranes, while the typical non-conductive substrates include polycellulose, plastic films, Kapton, silicone sheet, and paper, *etc.* The properties of the flexible substrate determine whether it is necessary to fabricate a current collector in electrode preparation. For example, a conductive substrate can also work as a current collector, while the use of a non-conductive substrate requires an additional conductive composite to be deposited or embedded into the substrate, working as a current collector. The substrate also determines the electrode preparation process. When metal foil, plastic or paper is used as the substrate, printing or painting can be used for electrode preparation, a process that can be readily scaled up for mass production. In this part, the flexible substrate and current collector will be emphasized in each selected example.

Metal foils, in terms of mechanical strength and flexibility (when thin enough), are one type of the optimal substrate for flexible LIBs. However, there are a number of drawbacks to using metal foils as a flexible substrate. First, the metal foils (*e.g.*, copper and iron for anodes and aluminum for cathodes) usually have densities relatively higher than other potential substrates. Using these foils would reduce the overall energy densities of a full LIB as the substrate would account for over 15% of the total mass of the electrode with no contribution to lithium storage.[18,51,52] Second, the metal foils have low surface areas, thus exhibit weak adhesion and limited contact to the active material. As such, gaps may be formed at the electrode–metal interface resulting from volumetric change of the active materials during the charge and discharge processes at higher rates. Thus, battery performances may undergo degradation both in capacity and cyclic stability. Such a problem becomes more concerning when preparing flexible batteries, as continuous deformation is more likely to result in detachment of active materials from the metal foils. Moreover, metal foils may not be chemically stable in electrochemical processes, and are susceptible to corrosion, leading to increased internal impedance, passivation of active materials and resulting in diminished capacity and rate capability.[53–55] As a result, limited

research has been conducted on the use of metal foils as flexible substrates; in contrast, carbon-based films and membranes are gaining research momentum.

Theoretically, carbon based materials are optimal substrates for flexible electrode as they can act as both current collector and active materials support. So far, many novel carbon 2D and 3D structures have been successfully fabricated, and some of them exhibit high flexibility and mechanical strength and have been studied as substrates/current collectors for flexible LIBs in lab scale. These include graphene paper, graphene foam, CNTs films, carbon cloth, and porous carbon films, *etc.*[44,53,56–68] Another kind of approach is to embed 1D nanostructured carbon (*e.g.*, CNTs) into polymer based films to produce a current collector and holds high potential for practical application.[69–78] In this part, we will first summarize the Type-I flexible electrodes in term of carbon assembly in the current collectors.

2.1.1 Flexible cathodes. Fabrication of flexible cathodes has been one of the major challenges in flexible LIBs research and development. One of the reasons is that the commonly used cathode materials, such as $LiCoO_2$, $LiMn_2O_4$, and $LiFePO_4$, are generally synthesized in high-temperature environments (>500 °C). Most flexible substrates or materials used to make flexible substrates are chemically unstable at these elevated temperatures. For example, although carbon is able to remain stable at temperatures higher than 1000 °C, it may react with cathode materials (*e.g.*, $LiCoO_2$ and $LiMn_2O_4$), leading to failure in obtaining optimal crystallinity, degradation of the cathode materials, and consequently lower battery performances. Typically the preparation of flexible cathode materials relies on deposition methods such as sputtering and laser ablation, where nanosized cathode materials can be successfully produced.[40,79,80] However, these processes are high cost and low efficiency. Therefore, inventing new processes for preparing flexible cathodes remains an important research topic.

I Conductive substrates. For conductive substrate supported flexible cathodes, CNTs thin films, carbon fibers thin films and graphene paper have been attempted for use as current collectors. Cui's research group did some pioneering studies.[56,57,78] In 2010, they reported a new structure of fully flexible LIBs using Xerox paper as a separator and free-standing CNTs thin films as cathode and anode current collectors.[56] The whole process is outlined in Fig. 1. The Xerox paper functioned as both a mechanically strong substrate and a separator membrane with lower impedance than commercial separators. For preparing the CNTs films, aqueous CNTs ink was prepared by dispersing commercial, arc-discharged CNTs in water with sodium dodecylbenzenesulfonate (SDBS) as a surfactant. The CNTs ink was then blade-cast onto a stainless steel (SS) substrate. The films have a low sheet resistance of ~5 ohm per sq, a weight of ~0.2 mg cm^{-2}, and excellent flexibility. Slurries of battery materials, $Li_4Ti_5O_{12}$ and $LiCoO_2$ were prepared by mixing 70 wt% active materials, 20 wt% Super P carbon, and 10 wt% polyvinylidene fluoride (PVDF) binder in *N*-methyl-2-pyrrolidone (NMP) as the solvent. The slurries with a thickness of ~125 μm were blade-coated on top of the previously prepared CNTs films that are still on the SS substrates and dried. The double layer $Li_4Ti_5O_{12}$/CNTs or $LiCoO_2$/CNTs films were formed on SS substrates. The double layer films easily delaminated from the SS substrate when gently shaken in water. For a full cell assembly, the $Li_4Ti_5O_{12}$/CNTs or $LiCoO_2$/CNTs films were laminated onto both sides of a Xerox paper. The whole assembly was subsequently sealed with a 10 μm polydimethylsiloxane (PDMS) film in an Ar-filled glove box using $LiPF_6$ in ethyl carbonate/diethyl carbonate (EC/DEC) as an electrolyte. The full battery assembly was measured to be ~300 μm thick. The anode and cathode mass loadings were calculated to be 7.2 and 7.4 mg cm^{-2}, respectively. After packaging, the battery exhibited robust mechanical flexibility (capable of bending down to <6 mm) and an energy density of 108 mW h g^{-1} full battery when cycling between 1.6 and 2.6 V. Initial Coulombic efficiency was measured to be 85%. Following the first cycle, Coulombic efficiency was calculated to be between 94 and 97%. The discharge retention was 93% after 20 cycles, as shown in Fig. 1.

In 2011, Baughman's group fabricated CNT biscrolled yarns and used them as a substrate for preparing cathodes containing $LiFePO_4$ contents of over 95 wt%.[58] The $LiFePO_4$@MWNTs biscrolled yarns cathodes were produced by filtration-based guest deposition and twist insertion in a liquid bath. Isopropanol was used as the liquid medium for the dispersion of the $LiFePO_4$ before filtration. Before electrochemical characterization, some samples of the obtained cathodes were thermally annealed at 600 °C for 6 hours in argon flow. As-prepared 1 to 2.5 cm long cathode fibers were employed as a complete cathode, without the need for the aluminum substrates and polymer binder. The electrochemical performance of the $LiFePO_4$ biscrolled yarns as a Li ion cathode was evaluated inside an argon-filled glove box using a three-electrode cell, which consisted of a $LiFePO_4$@MWNT4,6 yarn cathode, a graphite anode, and a lithium foil reference electrode. The electrolyte was 1 M $LiPF_6$ in PC–EC–DMC (1 : 2 : 3, v/v). The full batteries were cycled between 2.5 and 4.2 V at different rates. For a 100 mm diameter biscrolled yarn containing 95 wt% $LiFePO_4$ guest, which is weavable and knottable, the reversible charge storage capabilities based on total electrode weight are 115 mA h g^{-1} at C/3 rate and 99 mA h g^{-1} at 1 C (1 C = 170 mA h g^{-1}).

Recent publications utilizing CNTs thin films as a substrate have focused on half-cell flexible LIBs, and used lithium foil as a counter electrode. Wang, *et al.*, fabricated super-aligned CNTs films (SACNTs) as current collectors.[53] The SACNTs arrays with a tube diameter of 20–30 nm and a height of 300 μm were synthesized on silicon wafers by chemical vapor deposition (CVD) with iron as the catalyst and acetylene as the precursor. 20 layers of the SACNTs films were first cross-stacked onto a glass substrate for use as a current collector. An electrode slurry was prepared by mixing graphite or $LiCoO_2$, carbon black, and PVDF in NMP solvent at a weight ratio of 8 : 1 : 1. The electrode slurry was coated on top of the SACNTs current collector. After drying, the flexible and free-standing graphite–CNTs electrodes or $LiCoO_2$–CNTs electrodes were separated from the glass substrate. These electrode sheets were punched into circular discs with a diameter of 10 mm. The weights of graphite and $LiCoO_2$ in each disc were around 3–4.5 mg and 4.5–6.0 mg, respectively. CR 2016 half-cells were assembled with the

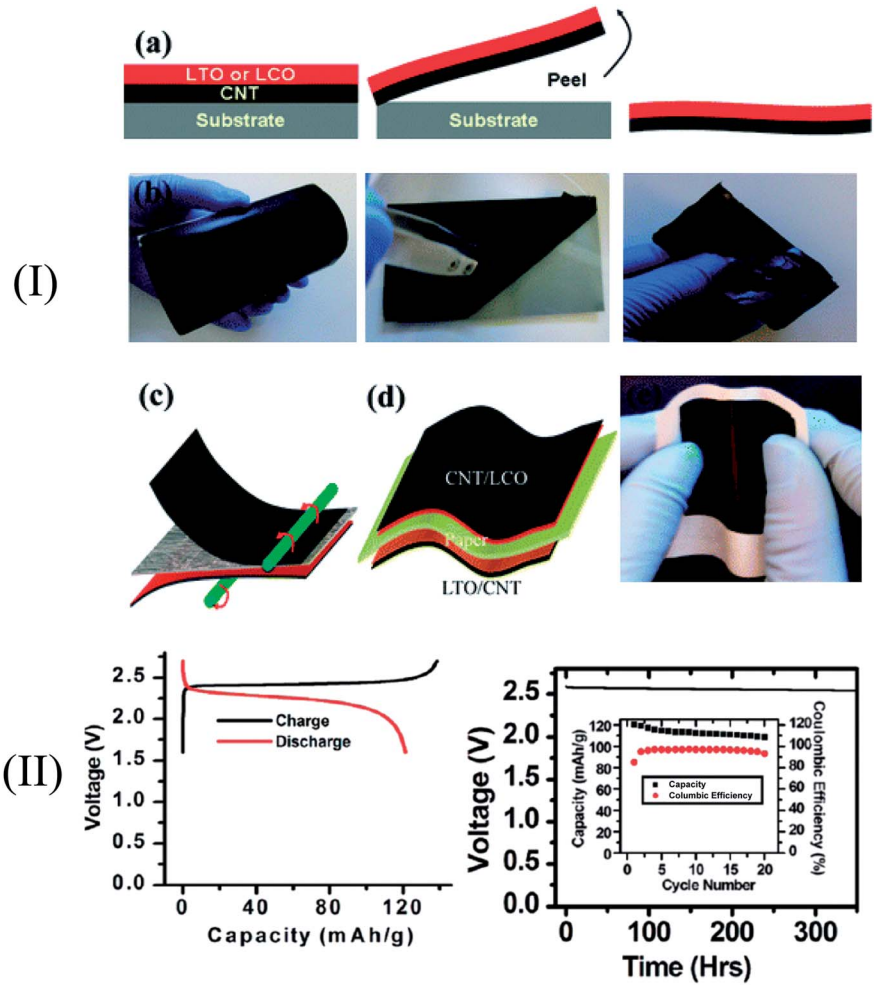

Fig. 1 (I) A schematic diagram of the fabrication process for free-standing $LiCoO_2$/CNTs or $Li_4Ti_5O_{12}$/CNTs double layer thin films and full battery assembly; and (II) electrochemical performance of a full battery tested between 1.6 and 2.6 V. Reproduced from ref. 56 with permission. Copyright 2010 American Chemical Society.

graphite–CNTs, graphite–Cu, $LiCoO_2$–CNTs, or $LiCoO_2$–Al discs as the working electrodes, and Li metal as the reference electrode. A porous polymer film (Celgard 2400) was used as the separator. A 1 M $LiPF_6$ in 1 : 1 EC and DEC solution was used as the electrolyte. The comparative study indicated that the $LiCoO_2$–CNTs cathode had the highest capacity. With a $LiCoO_2$ layer thickness of 57 μm, an energy density of ~478 W h kg^{-1} (normalized to cathode) was achieved when cycled between 3 and 4.3 V, displaying a 53% improvement over the $LiCoO_2$–Al electrode (312 W h kg^{-1}). Jia, *et al.*, reported a direct-growth method to produce high-performance flexible $LiMn_2O_4$–CNTs cathodes.[59] The group started with a flexible CNTs network that was mildly pre-oxidized. Spontaneous redox reactions between the CNTs and $KMnO_4$ generated layers of MnO_2 wrapping the CNTs. Subsequent hydrothermal treatment in the presence of LiOH converted the MnO_2/CNTs composites into $LiMn_2O_4$/CNTs composites. Vacuum filtration of the composites created free-standing cathodes that are binder-free and flexible. The produced electrodes had a thickness of 30–40 μm, with a $LiMn_2O_4$ weight ratio of 89% and nanocrystallite sizes between 50 and 100 nm. The electrical energy storage capability of the composite electrodes was examined in a coin-type half cell using lithium as both counter and reference electrodes. At a relatively high current density of 550 mA g^{-1} with cut-off voltages of 3.2–4.3 V, the composite material still delivered a discharge capacity of 50 mA h g^{-1} cathode.

Kercher, *et al.*, reported carbon fibers paper based cathodes.[60] Industrial carbon-bonded polyacrylonitrile (PAN) carbon fiber papers were used. The PAN fibers possessed excellent mechanical integrity, electrical and thermal conductivity. Coating slurries were created by mixing *N*-vinyl-2-pyrrolidone, AR mesophase pitch, and $LiFePO_4$ powder. During processing development, the pitch-to-powder ratio was kept constant (0.034), the weight percent of $LiFePO_4$ in the slurry being varied from 15 to 58 wt%. Swagelok cells were constructed with each carbon fibers paper cathode for battery testing with 26 and 41 wt% $LiFePO_4$, respectively. A cell was composed of lithium metal anode, a Celgard 2325 separator, a carbon fibers paper cathode, and approximately 2 mL of electrolyte solution containing 15 wt% $LiPF_6$, 25.5 wt% EC, and 59.5 wt% EMC. Constant current discharge tests were used to measure the discharge behavior (down to 2.5 or 2.8 V) and capacity (reported

for discharge only to 2.8 V) as a function of discharge current. The cathodes demonstrated capacities of ~170 mA h g^{-1} (~100% of theoretical capacity), when the crystallinity and size of $LiFePO_4$, the thickness of the substrate, and the loading of active materials matched well.

On the other hand, more full flexible LIBs were invented when graphene paper was successfully fabricated and was introduced into the LIBs. Due to the 2D assembly, graphene paper exhibits much higher mechanical strength than the 1D assembly of CNTs or carbon fibers does. Gwon, *et al.*, were the first reporting a new approach to make a full, flexible LIB based on free-standing graphene papers.[44] The battery was composed of cathode with V_2O_5 deposited on graphene paper, polymer separator (Celgard 2400), and anode with lithiated graphene paper, as shown in Fig. 2. Freestanding graphene papers of choice have a thickness of ~2 μm and a conductivity of ~8000 S m^{-1}. The cathode material V_2O_5 was grown on graphene paper by pulsed laser deposition (PLD) using a target prepared by cold pressing from a V_2O_5 powder and sintering at 600 °C in air. The thin films were deposited at room temperature in the presence of oxygen. To eliminate the undesired lithium uptake in the assembled cell from the first cycle irreversible reaction, the graphene paper anode was electrochemically lithiated to a potential of 0.02 V *vs.* Li prior to cell integration. For the full battery assembly, the V_2O_5/graphene paper cathode and the lithiated graphene paper anode were separated by a separator dipped in liquid electrolyte 1 M $LiPF_6$ in EC–DMC (1 : 1 by volume) and served as the electrolyte. The charge–discharge cycles of the assembled battery were measured between 3.8 and 1.7 V, at a constant current of 10 μA cm^{-2}. The battery performance shows the typical charge–discharge behavior of the amorphous V_2O_5 cathode. The first charge and discharge capacity were ~15 μA h cm^{-2}, with a negligible initial irreversible capacity.

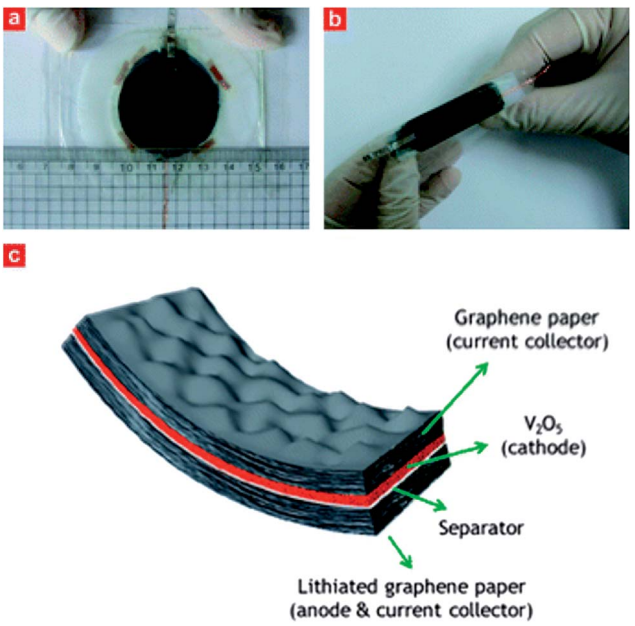

Fig. 2 An assembled flexible battery using V_2O_5/graphene paper as a cathode and a lithiated graphene paper as an anode. Reproduced from ref. 44 with permission. Copyright 2011 Royal Society of Chemistry.

Another type of graphene-based flexible battery design was recently demonstrated by Cheng's research group. The design consisted of $Li_4Ti_5O_{12}$ as the anode and $LiFePO_4$ as the cathode and exhibited ultrafast charge and discharge rates.[61] The battery assembly is schematically shown in Fig. 3. Graphene foam (GF) was used as current collectors, which consisted of a 3D interconnected network of high-quality CVD-grown graphene, and had an electrical conductivity of ~1000 S m^{-1}. The solid conductivity of the few-layer graphene itself within the GF is evaluated to be ~1.36 × 10^6 S m^{-1}. The GF was also extremely light (~0.1 mg cm^{-2} with a thickness of ~100 μm) and flexible. It possessed a high porosity of ~99.7% and a very high specific surface area and could be bent to arbitrary shapes without breaking. Chemical processing was used for electrode preparation. For the cathode, $LiFePO_4$ was synthesized from the hydrothermal reactions among $CH_3COOLi \cdot 2H_2O$, $Fe(NO_3)_3 \cdot 9H_2O$, and $NH_4H_2PO_4$ in the presence of GF. The as-prepared sample was heated at 720 °C under a hydrogen and argon atmosphere. For the anode, $Li_4Ti_5O_{12}$ was synthesized from the hydrothermal reactions among H_2O_2, LiOH, and Ti–$(OC_3H_7)_4$ in the presence of GF. The as-prepared sample was heated at 550 °C in argon. The graphene content in the $Li_4Ti_5O_{12}$/GF and $LiFePO_4$/GF electrodes was estimated to be ~12 wt%.

To complete the battery assembly, the free-standing $Li_4Ti_5O_{12}$/GF and $LiFePO_4$/GF electrodes, with a thickness of ~100 μm, respectively, were first laminated onto both sides of a polypropylene separator and then sealed with ~250 μm thick PDMS in an Ar-filled glove box using $LiPF_6$ in EC–DMC as the electrolyte. The total thickness of this flexible full battery was less than 800 μm. The flexible battery exhibited a charge–discharge plateau of ~1.9 V and an initial discharge capacity of ~143 mA h g^{-1} (full battery) with a Coulombic efficiency of 98% at a 0.2 C rate. Moreover, after 20 bends to a radius of 5 mm, only a negligible overpotential was observed, with a decrease of less than 1% compared to the original flat battery. The flexible battery showed capacity retention of ~97% after the first 15 cycles under a flat state, and ~95% after another 15 cycles under a bent state (a bend radius of 5 mm). This flexible full battery was also operated at a 10 C rate and obtained a capacity of 117 mA h g^{-1}. Furthermore, the flexible full battery can be cycled over 100 cycles at a high rate of 10 C with only 4% capacity loss. The related performances are shown in Fig. 3. This approach has a high potential for practical application if mass production of graphene foam is achieved.

Kwon, *et al.*, reported cable-type flexible full LIBs based on hollow multi-helix electrodes.[45] The battery design, shown in Fig. 4, comprised several electrode (generally anode) strands coiled into a hollow-spiral (helical) core and surrounded by a tubular outer electrode (cathode). With this architecture, the contact area between the anode and cathode is large and at the same time, the cell capacity and capacity balance between two electrodes can be tuned by adjusting the number of anode strands and the thickness of cathode composite. The battery fabrication had two major steps: (i) formation of the hollow-helix anode and (ii) assembly of other components of the cable

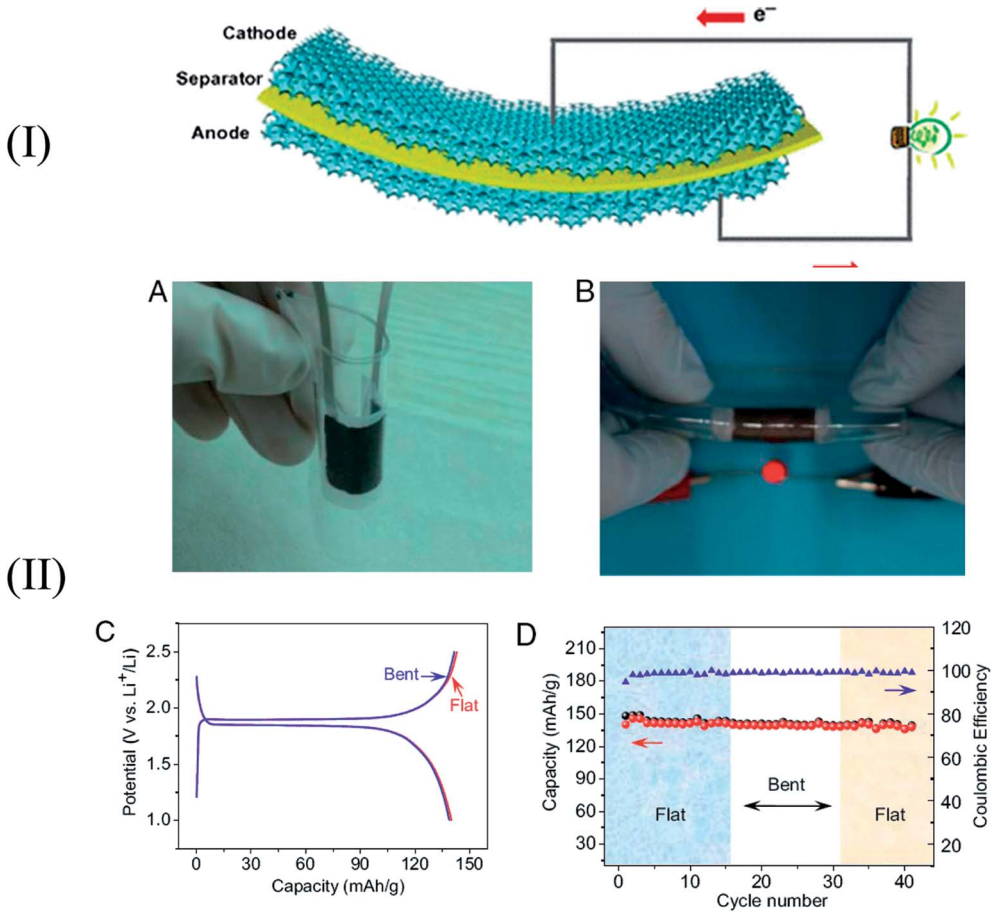

Fig. 3 (I) A schematic diagram of a flexible battery containing a $LiFePO_4$ cathode and a $Li_4Ti_5O_{12}$ anode made from 3D interconnected graphene foam; and (II) electrochemical performances of a full battery before and after deformation tested between 1.0 and 2.6 V. Reproduced from ref. 61 with permission. Copyright 2012 National Academy of Science.

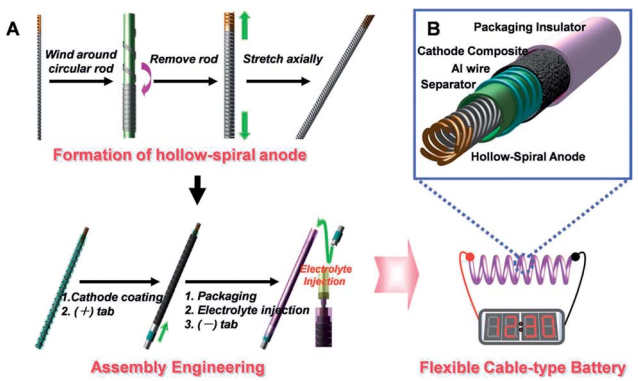

Fig. 4 A schematic diagram of the process for fabricating cable battery. Reproduced from ref. 45 with permission. Copyright 2012 WILEY-VCH Verlag GmbH & Co. KGaA, Weinheim.

battery. First, Ni–Sn active material was electrodeposited on a 150 μm diameter Cu wire. A twisted bundle was prepared with three strands of Ni–Sn-coated wire by a method that is usually used for producing yarn to achieve a certain degree of stiffness and maintain the hollow frame. Then the hollow-helix anode was fabricated by winding four of the twisted wire bundles around a circular rod and pulling axially so that the outer diameter of the anode was about 1.2 mm. After that, a modified poly(ethylene terephthalate) (PET) nonwoven support (separator) and an aluminum wire (cathode current collector) were wound in order around the hollow-helix anode. The slurry of the cathode was prepared by mixing $LiCoO_2$, acetylene black, and PVDF binder in an 8 : 1 : 1 mass ratio in NMP. The prepared anode/separator/Al wire assembly was coated with the slurry by drawing it through a coating bath followed by drying. A positive tab consisting of an Al plate and insulating tube was integrated at the end of the positive electrode. Then the electrode assembly was inserted into a heat-shrinkable tube and heated with a heat gun to shrink the tube so that the shrunken packaging insulator closely adhered to the outer surface of the electrode assembly. Finally, a liquid organic electrolyte, 1 M $LiPF_6$ in EC and PC (1 : 1 by volume) containing 3 wt% vinylene carbonate, was injected into the hollow space at the center of the electrode assembly and a negative tab comprising a Ni plate and insulating tube was attached to the end of the negative electrode. The capacities and cycle performances of the prepared cable batteries were examined by the following sequence: (i) the cable battery was charged to 4.2 V at a rate of 0.1 C (0.1 mA cm^{-1}) under constant current (CC) conditions and then maintained at

a constant voltage (CV) of 4.2 V. CV charging was terminated when the current dropped below 0.05 mA cm^{-1}. (ii) The cable battery was discharged to 2.5 V at a rate of 0.1 C under CC conditions. The cable battery with the hollow anode reversibly charged and discharged with stable capacity retention close to its designed cell capacity (per unit length of cable battery) of 1 mA h cm^{-1}. This is a complex battery design.

II Non-conductive substrate. When non-conductive substrates are used, a conductive layer must be embedded so as to work as a current collector. The current collectors are fabricated mainly by metal deposition and CNTs impregnation. Koo, *et al.*, developed a full flexible LIB based on all-solid-state materials under polymer sheet wrapping.[69] For the battery fabrication, a universal transfer approach based on sacrificial mica substrates was used. In detail, a Ni-based alloy was sputtered on layered mica and used as a current collector. A $LiCoO_2$ layer is consecutively stacked under argon gas on the current collector material as a cathode electrode by radio frequency (RF) magnetron sputtering with a $LiCoO_2$ sintered target, followed by HT treatment (700 °C) using a rapid thermal annealing (RTA) system. The deposition of a LiPON electrolyte film was carried out by RF magnetron sputtering with a Li_3PO_4 sintered target under pure nitrogen gas, and then Li metal, acting as an anode/current collector, was deposited by thermal evaporation in a glove box. The final fabrication step on the mica substrate involved the encapsulation process. The upper protective encapsulation layer prevented exposure of the LiPON solid electrolyte and Li anode materials to moisture or oxygen, which would accelerate the degradation of the battery performance. The mica substrate of the thin-film LIB was peeled off by physical delamination using sticky tapes. After substrate delamination, the flexible LIB was transferred onto a PDMS polymer substrate. Finally, the flexible thin-film LIB was wrapped with another PDMS sheet to enhance the mechanical stability. The structure of the flexible LIB is shown in Fig. 5. The LIB properties as a function of the bending radius (R_c) showed suitability for a high-performance flexible energy source. The flexible LIB was capable of a maximum 4.2 V charging voltage and delivered a capacity of 106 μA h cm^{-2}. This process is high cost and low efficiency.

Nojan reported flexible paper based current collector fabricated from wood microfibers that were coated with CNTs through an electrostatic layer-by-layer nano-assembly process.[70] The pulp was made from beaten, bleached Kraft softwood microfibers (less than 1% lignin and 99% cellulose), that were press-dried, and shipped in bundles of sheets. These hollow microfibers are 2–3 mm in length and 35–50 μm in diameter. An aqueous dispersion of poly(3,4-ethylenedioxythiophene)–poly(styrenesulfonate) (PEDOT–PSS) conductive polymer and CNTs was used as the anionic component, while poly(ethyleneimine) (PEI) was used as cationic polyelectrolyte component for the layer-by-layer coating of the wood microfibers.

Coating microfibers with two bilayers of PEI/CNTs in alternate with one bilayer of PEI/PEDOT–PSS achieved the desired conductivity. The CNTs mass loading was 10.1 μg cm^{-2}. Following CNTs-coating, the wood microfibers were assembled into flexible paper sheets for use as current collectors. Pastes of the electrode materials were prepared using 85 wt% of the active materials ($Li_4Ti_5O_{12}$ or $LiCoO_2$), 10 wt% Super P carbon, and

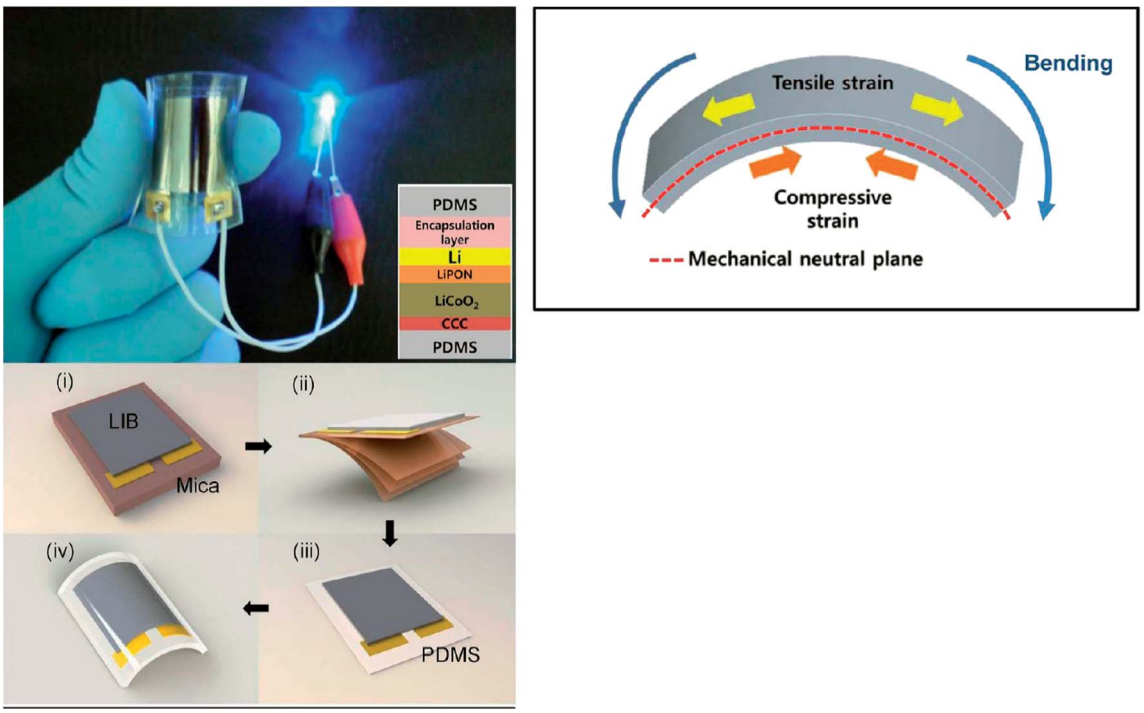

Fig. 5 A schematic diagram of the process for fabricating a fully flexible LIB based on all-solid-state materials ($LiCoO_2$ as a cathode, LiPON as an electrolyte, and Li film as an anode, respectively) under polymer sheet (PDMS) wrapping. Reproduced from ref. 69 with permission. Copyright 2012 American Chemical Society.

5 wt% PVDF. The electrode materials were then coated on the current collectors by a spray coating method followed by vacuum-drying. For electrochemical test, the CNTs–microfiber paper, coated with $Li_4Ti_5O_{12}$ and $LiCoO_2$, were cut in circular samples with diameter of 0.58 cm, which formed the anode and cathode of the developed battery. A Celgard separator was used. The outer surfaces of the CNTs–microfiber current collectors were connected to the output of the battery. The battery assembly was soaked in 1 M $LiPF_6$ in an EC–DEC electrolyte solution (1 : 1 by volume), pressed, and encapsulated in a coin cell. The $Li_4Ti_5O_{12}$ and $LiCoO_2$ half-cells with CNT–microfiber paper current collectors were tested between 0.5 and 1.8 V and 3.5 to 4.3 V, respectively. The full-cells with $Li_4Ti_5O_{12}$ and $LiCoO_2$ electrodes on CNT–microfiber paper current collectors were tested for charging–discharging performance between 1.2 V and 2.7 V. The capacities of the batteries made with the current collectors were 150 mA h g^{-1} for the $LiCoO_2$ half-cell, 158 mA h g^{-1} for the $Li_4Ti_5O_{12}$ half-cell, and 126 mA h g^{-1} for the $Li_4Ti_5O_{12}/LiCoO_2$ full-cell.

One of the most recent related researches was reported by Petrov's group, who provided a very complex design of flexible batteries.[71] As shown in Fig. 6, the device was arrays of small-scale LIBs that were connected by conducting frameworks with extraordinary stretchable characteristics. The current collectors consisted of photolithographically patterned circular disks of Al (600 nm thick) and Cu (600 nm thick). The overall construct consisted of a square array of 100 electrode disks, electrically connected in parallel. Experimental detail is shown in ref. 71. Moulded pads of slurries based on $LiCoO_2$ and $Li_4Ti_5O_{12}$ served as active materials at the cathode and anode. The slurry materials were composed of $LiCoO_2$ or $Li_4Ti_5O_{12}$, acetylene black and polyvinylidene fluoride, mixed in a weight ratio of 8 : 1 : 1 in a solvent of NMP for the cathode and anode, respectively. The mixture was mechanically scraped across the etched surface of the silicon wafer, so that the cylindrical wells in the wafer were filled with slurry. The two sheets laminated together in a way that involved spatial offsets between the active materials to avoid electrical shorts between them and to eliminate the need

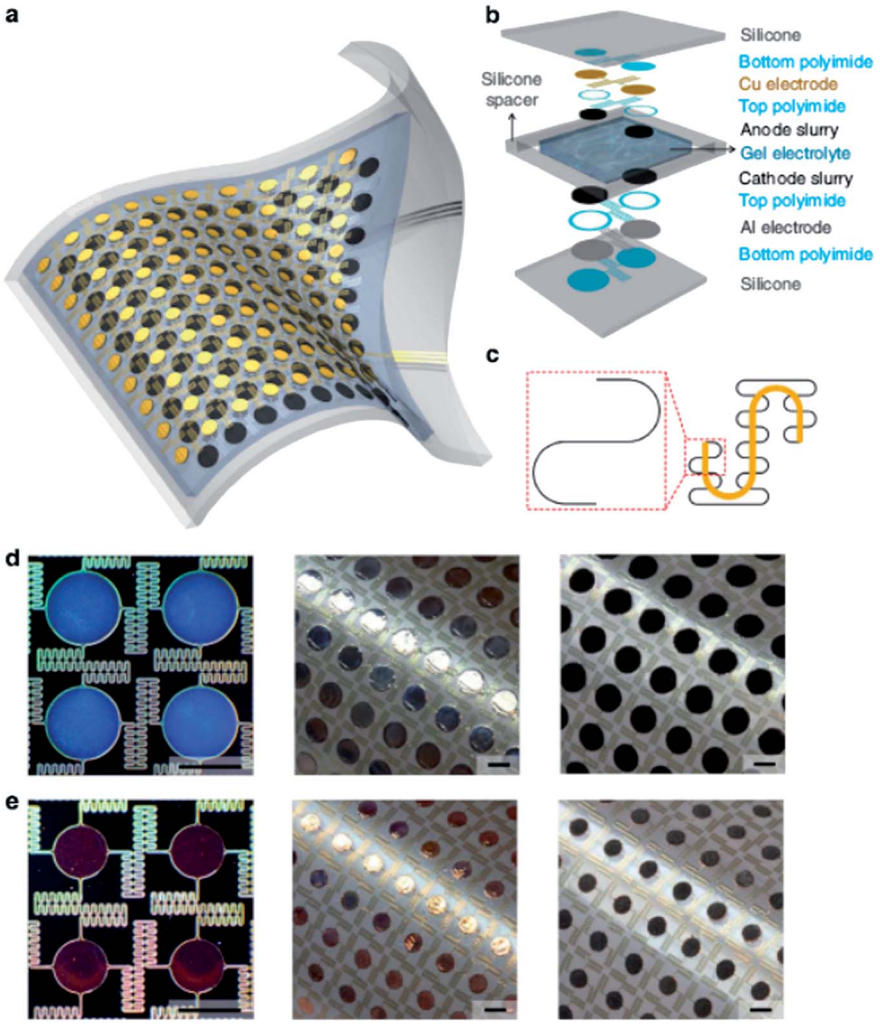

Fig. 6 A schematic diagram of the process for fabricating the devices with arrays of small-scale LIBs (with $LiCoO_2$ and $Li_4Ti_5O_{12}$ as cathode and anode materials, respectively) that are connected by conducting frameworks. Reproduced from ref. 71 with permission. Copyright 2013 Nature Publishing Group.

for a separator. A spacer, made of the same silicone elastomer and applied around the periphery of the system, prevented direct contact of the top and bottom sheets. A gel electrolyte injected into the gap provides media for ionic transport. Thin encapsulating layers of an acryloxy perfluoropolyether elastomer bonded to the outer surfaces helped to prevent moisture from diffusing into the battery and solvents in the gel from leaking out.

The as-fabricated and stretched battery electrodes and the cycling behaviour of the full, integrated battery were tested at a cut-off voltage of 2.5–1.6 V at room temperature. The result enabled reversible levels of stretchability up to 300%, while maintaining capacity densities of ~1.1 mA h cm^{-2}.

2.1.2 Flexible anodes. As compared to cathodes, much more research has focused on flexible anodes. This is probably due to (1) the ease of materials handling, and (2) the configuration effectively accommodating the large volumetric expansion of Si and Sn. The studies, according to the substrate/current collector, can also be categorized as flexible anode with active materials deposited on conductive substrates (carbon films or metal strips) and flexible anode with active materials deposited on non-conductive substrates. It is worth mentioning (1) some studies reviewed in the forementioned flexible cathodes also made novel design of various such type of anodes.[56,61,69–71] To avoid repetition, in this part, we will select several other representative anode systems to demonstrate the science and technology; and (2) the carbon based substrate may also contribute to lithium storage. This issue is not specially addressed in the existing studies on electrode materials evaluation.

I Conductive substrates. Liu, *et al.*, reported the synthesis of a hierarchical silicon NWs–carbon textiles matrix as a novel flexible anode for LIBs.[62] Silicon NWs were synthesized *via* a CVD process and were dispersed in ethanol by sonication to form a homogeneous slurry. Cleaned carbon textiles were subsequently coated with prepared Si NWs slurry with a loading density of 2.4–3.5 mg cm^2. Finally, 3D Si NWs–carbon textiles matrix was achieved by a facile spray-coating approach. Full flexible LIB was assembled using the prepared Si NWs–carbon textiles anode, commercial $LiCoO_2$ cathode, Celgard 2400 separator, and $LiPF_6$-based electrolyte. For the full batteries, the capacities of cathode ($LiCoO_2$) and anode (Si) were approximately 10–12 and 2.1–3.4 mA h, and thus these $LiCoO_2$ cathodes just worked as a counter electrode and the as-assembled full batteries are anode-limited units. The full battery demonstrated specific capacities of ~1580 mA h g^{-1} at 0.2 C (1 C = 4200 mA h g^{-1}) when cycled at 2.5–4.0 V, a good repeatability/rate capability (~950 mA h g^{-1} at 5 C), a long cycling life, and an excellent stability in various external conditions (curvature, temperature, and humidity), as shown in Fig. 7.

Using carbon cloth as templates, Liu, *et al.*, fabricated hierarchical $ZnCo_2O_4$ nanowire arrays/carbon cloth anodes by two-step hydrothermal treatments.[63] $ZnCo_2O_4$ NWs were produced using $Zn(NO_3)_2 \cdot 6H_2O$, $Co(NO_3)_2 \cdot 6H_2O$, NH_4F, and $CO(NH_2)_2$ as precursors. The reactant solution, along with carbon cloth, was transferred into a Teflon-lined stainless steel autoclave. The loading density of $ZnCo_2O_4$ was calculated to be 0.3–0.6 mg cm^{-2}. The final flexible battery consisted of produced $ZnCo_2O_4$/carbon cloth as the anode and commercial $LiCoO_2$ as the cathode. Aluminum and nickel were used as current collectors and attached to the cathode and anode electrode, respectively.

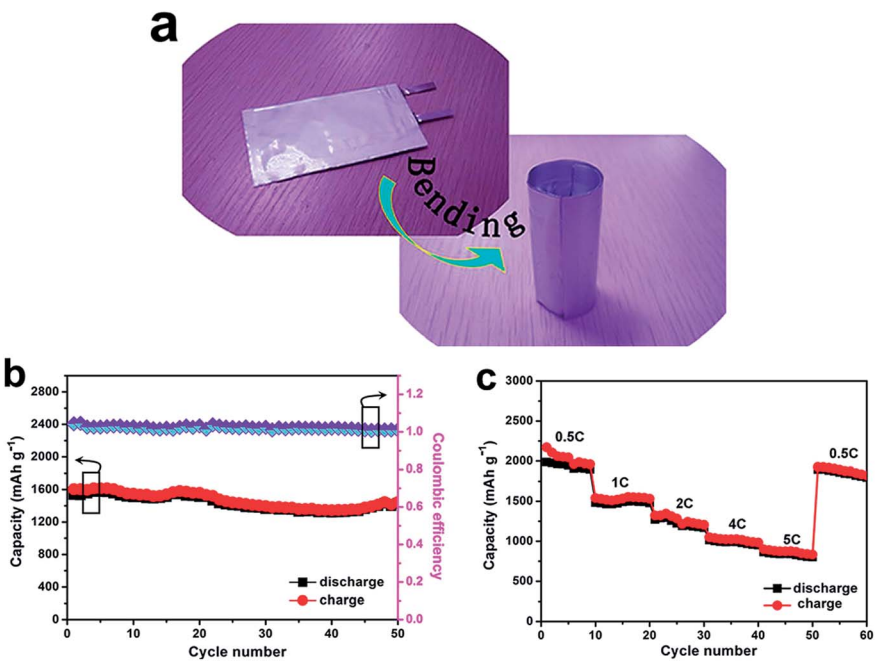

Fig. 7 (a) A full flexible Li-ion battery composed of Si NWs–carbon textiles anode, commercial $LiCoO_2$ cathode, Celgard 2400 separator, and $LiPF_6$-based electrolyte, (b) and (c) cyclic stability and rate capability. Reproduced from ref. 62 with permission. Copyright 2013 Nature Publishing Group.

An aqueous solution of 1.05 mol L^{-1} $LiPF_6$ in a mixture of EC and DMC (v/v = 1 : 1) served as the electrolyte along with a Celgard 2400 membrane separator. The final assembly was produced using an edge bonding machine with flexible plastic bags, as schematically shown in Fig. 8. The $ZnCo_2O_4$ NWs arrays/carbon cloth anodes exhibit high reversible capacities and excellent cycling ability. The cycling performance of a $ZnCo_2O_4/LiCoO_2$ battery was tested between 2.2 and 3.7 V at a current density of 200 mA h g^{-1}. The reversible capacity of the flexible device maintained a nearly constant value of approximately 1300 mA h g^{-1} (anode) and still kept about 96% of the initial capacity even after 40 cycles. In addition, Coulombic efficiency for this device sustained a constant value of 97–99% throughout cycling.

Some similar studies focused on testing the anodes in half-cell batteries. Liu, *et al.*, reported 3D conductive network anode electrodes based on commercial nickel foam current collector supported Si NWs with carbon coating.[64] A cleaned Ni foam was completely immersed in Si NWs solution to obtain a piece of Ni foam with fully absorbed Si NWs. The silicon loading could reach 5 mg cm^{-2}, with no use of binders. For carbon coating, the pressed Si NWs–Ni foam was completely immersed in a saturated glucose solution followed by annealing under a H_2–Ar atmosphere. For electrochemical testing, standard CR2032 coin cells were assembled with the pressed Si NWs–Ni–C foam as the working electrode and Li foil as the counter electrode. 1.0 M $LiPF_6$ in solution of 1 : 1 (w/w) EC–DEC was used as electrolyte. The cyclic performance was tested between 0.01 and 2 V. The resultant anode exhibited an initial capacity of ~2486 mA h g^{-1} (anode). A reversible capacity of 1500 mA h g^{-1} was still retained even after 50 cycles.

Choi, *et al.*, fabricated patterning of electrodes for mechanically robust and bendable LIBs. 3D nanostructured CuO nanoflakes were grown on the patterned Cu foils *via* a simple solution immersion process.[65] Silicon nanoparticles were filled into the patterned Cu current collectors. The strong anchoring of the nanostructured CuO materials to the patterned Cu foils remained unchanged even after 100 bending cycles, resulting in high electrochemical performances, including a high reversible capacity (~550 mA h g^{-1} anode after 100 cycles) and a high rate capability (220 mA h g^{-1} at a rate of 10 C at cut-off voltages of 0.005–3 V). Liu, *et al.*, prepared flexible anodes with silicon NPs supported in CNTs paper by low energy ion implantation.[67] Total dose of Si was ~1×10^{20} atoms cm^{-3}. The cells were tested at 25 mA g^{-1} between 0.01 and 2 V with Li foil as a counter electrode and 1 M $LiPF_6$ in EC and DEC (1 : 2, v/v) as an electrolyte, respectively. The implanted Si can improve the specific capacity and the reversible capacity of CNTs paper. After 50 cycles, the specific capacity of Si-implanted CNTs paper was 30% higher than the pristine CNTs.

Bradford's research group reported aligned CNTs–Si sheets as a novel nano-architecture for flexible LIBs electrodes.[66] CNTs forests were grown on a quartz substrate using iron chloride ($FeCl_2$) as the catalyst and C_2H_2, Ar, and Cl_2 as the reaction gases. A 10-layer CNTs sheet (2 mg cm^{-3}) was placed onto a quartz substrate for CVD deposition of silicon. The silicon coated CNTs sheet was further coated with carbon by a CVD process. Working electrodes were prepared by punching the as-prepared films directly into disks with a diameter of 0.5 inch. Neither binder nor current collector was used for preparing the electrodes. Typical electrode mass was 0.4–0.5 mg. The counter electrode was lithium ribbon. The electrolyte was 1 M $LiPF_6$/EC + DMC + DEC (1 : 1 : 1 by volume). 2032 coin cells were

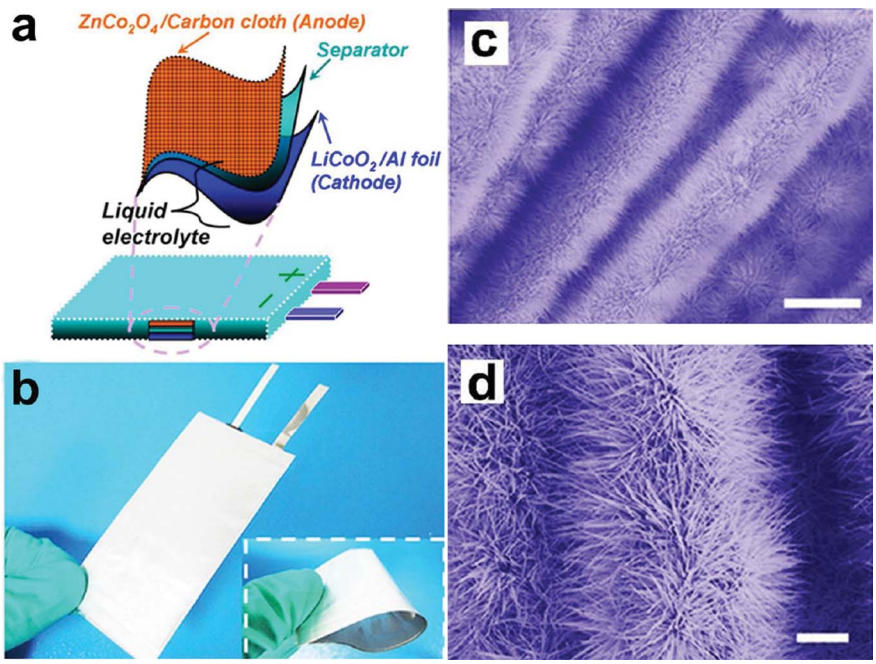

Fig. 8 A schematic diagram of the process for a full flexible LIB with hierarchical $ZnCo_2O_4$ nanowire arrays/carbon cloth as an anode and $LiCoO_2$ as a cathode. Reproduced from ref. 63 with permission. Copyright 2012 American Chemical Society.

assembled in an Ar-filled glove box. All cells were tested with cut-off potentials between 0.01 and 1.0 V. At 100 mA g^{-1}, the CNTs–Si–C sheet anodes exhibited charge capacity of 1494 mA h g^{-1} (anode) after 45 cycles with a capacity retention of over 94%. The Coulombic efficiency for each cycle was stabilized above 98%. At higher rates, *i.e.*, 200, 400, and 800 mA g^{-1}, the capacities were maintained at ~1500, 1250, and 1000 mA h g^{-1} with a slight decrease in Coulombic efficiency as the current density increased.

II Non-conductive substrates. Cheng, *et al.*, reported folding paper-based LIBs for higher areal energy.[72] Laboratory Kimwipes were used as substrates due to their thin and porous nature, which allowed for the CNTs ink to diffuse easily both inside and outside of the wipe. The Kimwipes was soaked in the CNTs ink solution to ensure that the CNTs would be distributed uniformly on the surface and within the paper pores. After soaking the Kimwipes with CNTs ink solution, the substrate was heated with a heat gun. The soaking and drying process was repeated several times followed by washing to obtain a sheet resistivity of ~5 Ω sq^{-1}. Another kind of CNTs–PVDF coated papers was also prepared in a similar process. Full cells were prepared using $Li_4Ti_5O_{12}$ and $LiCoO_2$ powders deposited onto the CNTs coated papers. The slurries were prepared by mixing the active materials, carbon black and PVDF binder with a ratio of 8 : 1 : 1.3 by weight. The slurry was uniformly coated on the CNTs-coated paper using doctor blading, and was followed by drying. A piece of Cu or Al foil was used as metal backing layer to supplement the CNTs/PVDF-coated paper current collector. The full battery was composed of $Li_4Ti_5O_{12}$/CNTs/PVDF-coated paper as anode, monolayer polypropylene (Celgard 2500) as a separator, and $LiCoO_2$/CNTs/PVDF-coated paper as cathode. Cu and Al foils were used as additional current collectors and the cells were sealed in aluminized polyethylene (PE) bags as pouch cells. The full batteries were cycled between 1.0 and 2.7 V. Folded cells showed higher areal capacities compared to the planar versions with a 5 × 5 cell folded using the Miura-ori pattern displaying a 14× increase in areal energy density, *i.e.*, 1.4 mA h cm^{-2} *vs.* 0.1 mA h cm^{-2}, as shown in Fig. 9.

Earlier, Wang, *et al.*, reported flexible and highly conductive SWCNTs/polycellulose papers (SWCNTs/PPs) developed for use as current collectors by a similar process.[73] PP was cut to desired sizes and dipped into CNTs ink followed by drying. This process was repeated 10 times to ensure that the polycellulose paper has been completely saturated with CNTs. Slurries of electrode materials, $Li_4Ti_5O_{12}$, $LiFePO_4$ and anatase TiO_2 nanosheets, were prepared by mixing 70 wt% active materials, 20 wt% Super P Carbon and 10 wt% PVDF binder in NMP as solvent. The conductive SWCNTs/PPs were immersed into the electrode slurries and immediately taken out after soaking. CR 2016 coin full cells were made using $Li_4Ti_5O_{12}$ and $LiFePO_4$ electrodes based on SWCNTs/PPs, Celgard 2400 as the separator and an electrolyte consisting of 1.0 M $LiPF_6$ in 1 : 1 w/w EC–DEC. The charge and discharge measurement of full cells using $Li_4Ti_5O_{12}$ and $LiFePO_4$ electrodes based on SWCNTs/PP conductors was carried out in a potential range from 1.4 to 2.6 V (*versus* Li) at different rates. They showed a first discharge capacity of 153.5 mA h g^{-1} with Coulombic efficiencies of 90.6% at 0.1 C and discharge capacity of 102.6 mA h g^{-1} at high rate (10 C).

Choi, *et al.*, reported silicon nanofibrils on a flexible current collector for bendable LIB anodes.[74] The flexible current collector was prepared using a Celgard 2400 separator as a substrate. The surface of the separator was treated with O_2 plasma to enhance roughness and adhesion of the copper layer. Copper and silicon were consecutively sputtered onto the treated substrate by RF-magnetron sputtering to form the flexible current collector and flexible silicon anode, respectively. The surface resistance of the copper layer was found to be inversely proportional to the layer thickness. When the copper layer thickness exceeded 230 nm, a surface resistance of less than 1 Ω sq^{-1} was obtained. For battery assembly, lithium metal was used as a counter electrode with 1 M $LiPF_6$ in 1 : 1 (v/v) EC–DEC as an electrolyte solution. The polyethylene separator was soaked in electrolyte prior to cell assembly. The cells were sealed in aluminized polyethylene laminate bags. The charge–discharge cycling properties were measured in a voltage region of 0.005–1.5 V under a constant current condition. The electrode exhibited energy capacities over 2000 mA h g^{-1} (normalized to Si) during 30 charge–discharge cycles at C/2. In addition, the Coulombic efficiency remained over 99% after the third cycle.

In 2012, Vlad, *et al.*, reported roll up nanowire battery from silicon chips.[75] In this approach, both electrode preparation and full battery assembly are complex and costly. The full battery is schematically shown in Fig. 10. Vertically aligned Si NWs etched from recycled silicon wafers were captured in a polymer matrix that operated as Li^+ gel-electrolyte and electrode separator and peeled off to make multiple battery devices out of a single wafer. Porous, electrically interconnected copper nanoshells were conformally deposited around the silicon NWs to stabilize the electrodes over extended cycles and provided efficient current collection. For full cell measurements, the cathode was made of $LiCoO_2$, carbon black and PVDF binder in a weight ratio of 85 : 10 : 5. The slurry was prepared by stirring the above mixture of $LiCoO_2$, carbon black and PVDF in NMP thoroughly, followed by casting onto a LIPOSIL composite film. After vacuum drying the resultant structures, an Al thin film was coated by sputtering to serve as a cathode current collector. The full cells were soaked in 1 M solution of $LiPF_6$ in 1 : 1 (v/v) mixture of EC and DMC for 1 h prior to the electrochemical studies. When galvanostatically cycled between 2.8 and 4 V, the cell delivered an initial capacity

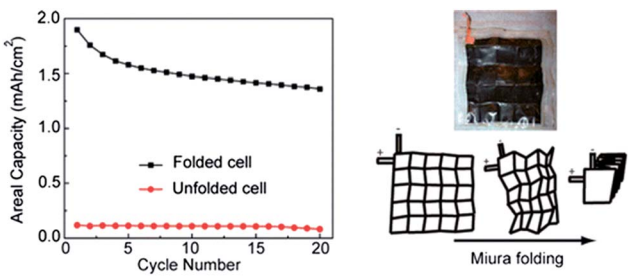

Fig. 9 A schematic diagram of folding paper-based LIBs consisting of $Li_4Ti_5O_{12}$ and $LiCoO_2$ powders deposited onto the CNTs coated papers and the performances of folded and unfolded cell. Reproduced from ref. 72 with permission. Copyright 2013 American Chemical Society.

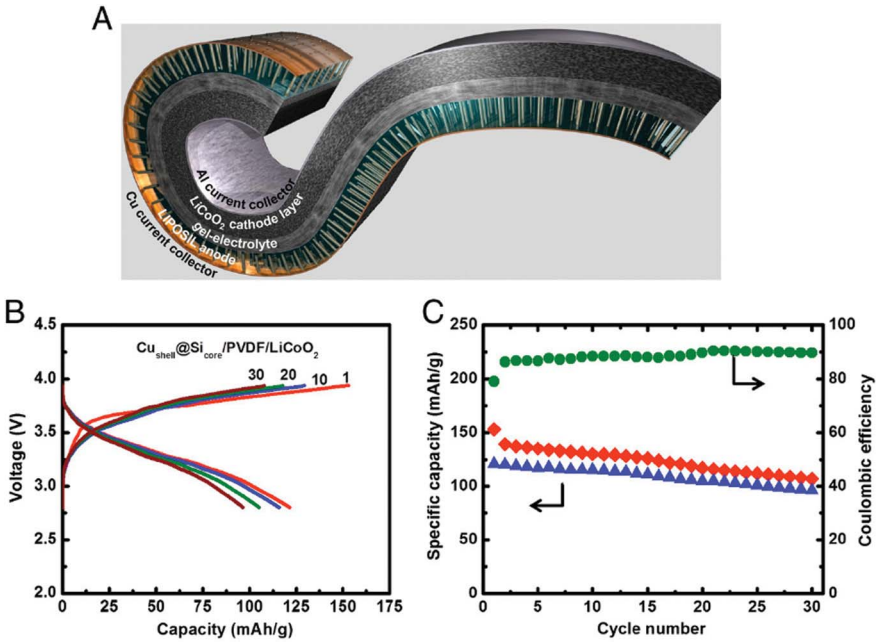

Fig. 10 3.4 V LIPOSIL with composite NW anodes. (A) Schematic view of the rolled LIPOSIL full cell architecture. (B) Charge-discharge profiles for the LIPOSIL battery with a spray coated $LiCoO_2$ cathode layer onto the assembled Si NWs-polymer composite. (C) Cycling performance and Coulombic efficiency of the LIPOSIL full cell, cycled between 4 and 2.8 V at a current rate of C/20 (capacity is given with respect to weight of $LiCoO_2$).

of 155 mA h g^{-1} at a current rate of C/20 (C-rate defined as 1 C = 1 h to discharge). The battery operated at an average voltage of 3.4 V with little capacity decay for the first 30 cycles. The first cycle Coulombic efficiency was ~80% and following cycles around 90%.

2.2 Free-standing electrodes (Type-II)

Free-standing flexible electrodes are generally assemblies of 1D and 2D nanostructured active materials involving nanostructured carbon (such as graphene, CNTs, carbon fibers), Si NWs and NPs, metal oxide NWs and NPs, *etc.* Most of the assemblies are achieved *via* a filtration process. Low efficiency is a biggest drawback that may prevent the practical application of such flexible electrodes. Their relatively lower mechanical strength is also a concern. As such, such flexible electrodes are still in laboratorial study and there are few full battery constructions.

2.2.1 Free-standing cathodes. Lukman developed bendable LIBs with paper-like free-standing V_2O_5–polypyrrole as cathodes. The flexible cathodes were prepared by vacuum filtration.[81] A modified hydrothermal method was used to control the length of V_2O_5 NWs for the preparation of free-standing films. The V_2O_5–PPy composite was prepared by polymerization of pyrrole monomer in the presence of V_2O_5 NWs. To ensure the production of a uniform film, the V_2O_5–PPy material was dispersed into Triton X-100 surfactant by ultrasonication. The as-prepared suspension was filtered under vacuum. The resultant mat with its PVDF membrane was washed by ethanol and dried and then the membrane was peeled off. For full battery assembly, a gel electrolyte was synthesized from poly(vinylidenefluoride-*co*-hexafluorpropylene) P(VDF-HFP), NMP and 30 nm Al_2O_3 powders. The gel electrolyte slurry was cast onto the surface of the freestanding V_2O_5–PPy electrode and dried under vacuum. After evaporation of the NMP, the electrode with gel electrolyte precursor was soaked in a conventional electrolyte solution of $LiPF_6$/EC–DMC. The electrode with gel electrolyte was fabricated into flexible bendable cells with lithium foil as the counter-electrode. Flexible and soft aluminium laminated pack materials were used to assemble the bendable cells. Fig. 11 contains a schematic diagram of a typical flexible and bendable cell. The battery performance of the repeatedly bent cell was similar to that of the conventional cell. The V_2O_5–PPy film delivered a significantly higher reversible capacity than the pristine V_2O_5 film and an excellent cycling stability (187 mA h g^{-1} cathode

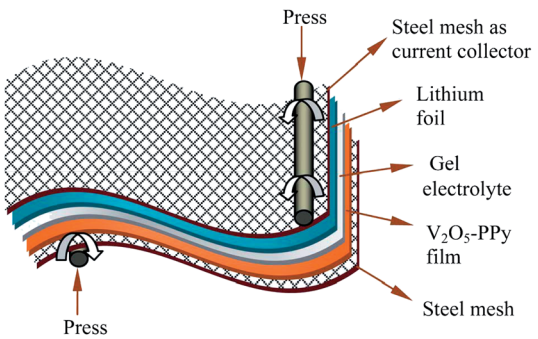

Fig. 11 A schematic diagram of a full flexible LIB with paper-like free-standing V_2O_5–polypyrrole as a cathode and a lithium foil as an anode. Reproduced from ref. 81 with permission. Copyright 2012 Royal Society of Chemistry.

when cycled between 1.5 and 4.0 V at a constant current of 40 mA g^{-1} after 100 cycles). Similarly, Qian, *et al.*, prepared free-standing, flexible V_2O_5–graphene composite films by simple filtration of aqueous dispersions of V_2O_5 NWs and graphene sheets.[82] V_2O_5 NWs were preferentially oriented along the plane of the film as they were sandwiched between stacked graphene sheets in the composite film. The V_2O_5 content in the composites was adjusted simply by varying the relative amount of the dispersions. Thermal annealing at 300 °C increased the conductivity of the composite films. Electrochemical cycling was conducted in a voltage range from 2.1 V to 4.0 V (*vs.* Li/Li^+) and a rest time of 5 min before each discharge and charge step. In binder-free, sandwich-type LIB cells, a composite film containing 75.8 wt% V_2O_5 delivered discharge capacities of 283 mA h g^{-1} and 252 mA h g^{-1} cathode at a current density of 50 mA g^{-1} during the first and 50th cycles, respectively. A composite film containing 42.8 wt% V_2O_5 delivered a discharge capacity of 189 mA h g^{-1} at 750 mA g^{-1} because of the presence of more graphene and hence a higher electrical conductivity.

Ding, *et al.*, reported 3D graphene/$LiFePO_4$ nanostructures (GLFP) used as cathode materials for flexible LIBs.[83] The flexible GLFP electrodes were fabricated by a facile solvent evaporation process. In a typical procedure, 90% GLFP composites and 10 wt% PVdF were mixed together in a beaker with NMP as a solvent and subsequently dried under vacuum. Flexible electrodes were prepared by peeling off from the bottom of the beaker. The electrode thickness was kept constant at 200 μm. Prior to cell assembly, the flexible electrodes were bent symmetrically with a bending angle of 45°, 90° and 120° and repeated for 100 times, respectively. Test cells were assembled with the flexible GLFP as a cathode, lithium metal as an anode and Celgard 2300 film as a separator. An electrolyte of 1 M $LiPF_6$ dissolved in EC + DMC (1 : 1, v/v) was used. Charge/discharge experiments were performed at 25 °C in the voltage range of 2.4–4.2 V. The graphene/$LiFePO_4$ nanostructures showed high electrochemical properties and significant flexibility. The composites with low graphene content exhibited a high capacity of 163.7 mA h g^{-1} at 0.1 C and 114 mA h g^{-1} at 5 C with no addition of conductive agents.

2.2.2 Free-standing anodes. Free-standing anode electrodes have attracted a great deal of attention in the field of advanced materials research due to their ease of fabrication and wide variety of nanostructures of potential anode materials. Furthermore, most of these nanostructures typically employ an alloying process during lithiation as opposed to an intercalation mechanism. According to the composition, the free-standing anodes can be categorized as anodes with carbon in 2D or 3D assembly and hybrid anodes from assembly of carbon and high-capacity nanomaterials.

I Anodes with carbon in 2D or 3D assembly. Besides use as current collectors in flexible electrodes, the 2D and 3D carbon assembly, such as graphene paper, CNTs films, or graphene–CNTs composites, are tested directly as flexible anodes for LIBs.[84–100] Landi, in 2008, studied the lithium ion storage capacities of SWCNTs paper electrodes. Treated SWCNTs were filtered to form a free-standing SWCNTS paper.[93] These SWCNTs papers (each with a mass of ~1 mg) were assembled into a two-electrode electrochemical cell and tested in an Ar glove box. Lithium ribbon was applied on the opposite stainless steel electrode from the SWCNTs paper with an electrolyte-soaked Celgard 2325 spacer in between. An electrolyte was freshly prepared by using 1 M $LiPF_6$ in a solvent mixture containing a combination of EC, PC, and DMC. The free-standing SWCNTs electrode with this electrolyte combination demonstrates enhanced cyclic stability, retaining >95% of the initial capacity after 10 cycles. Galvanostatic cycling was performed at room temperature from 3 V to 0.005 V (*vs.* Li/Li^+). At a current of 372 mA g^{-1}, the purified SWCNTs papers exhibit reversible lithium ion capacities between 250 and 300 mA h g^{-1} anode. Later, Liu's group studied the electrochemical performances of CNTs paper made from three different types of commercial CNTs, *i.e.*, single-walled, double-walled, and multi-walled.[87] The conductive CNTs films were prepared by adding the CNTs to the starting dispersion of carbon black and Triton X-100, followed by vacuum filtration. Test electrochemical cells were assembled using the free-standing CNTs films as the working electrode and Li metal as both the counter and reference electrode. The electrodes were separated by a 1 mm thick glass-fiber separator saturated with 500 μL of electrolyte solution, 1 M $LiPF_6$ in EC–DMC in 1 : 1 mass ratio. The cells were galvanostatically charged and discharged between 0.01 and 2.00 V *vs.* Li/Li^+, at a constant specific current of 25 mA g^{-1}. The films based on multi-wall CNTs (MWCNTs) displayed much better electrochemical performance (175 mA h g^{-1} at a rate of 10 C (1 C-rate is defined as 300 mA g^{-1})) compared to films produced using single-wall and double-wall CNTs. Recently, Sun's research group developed a novel flexible nanoporous CNTs film that was used as flexible anode for LIBs, as shown in Fig. 12.[94] The CNTs film was prepared by a vacuum filtration method on a Celgard 3500 polypropylene separator. A coin-type electrochemical half-cell included a prepared electrode as the working electrode and a lithium foil as the counter electrode. The electrolyte was composed of 1 M $LiPF_6$ salt dissolved in EC–DEC–EMC in a 1 : 1 : 1 volume ratio. Electrochemical testing indicated that the assembled cell could reach a specific capacity up to 378 mA h g^{-1} when cycled between 0.01 and 3 V.

Wang, *et al.*, first reported chemically prepared graphene paper exhibiting distinguishable electrochemical properties.[84] The graphene papers from vacuum filtration were mechanically strong and electrically conductive with Young's modulus of 41.8 GPa, tensile strength of 293.3 MPa, and conductivity of 351 S cm^{-1}. The first discharge for this electrode exhibited a consistent flat plateau and a discharge capacity of 528 mA h g^{-1} with a cutoff voltage of 2.0 V. The midpoint of the discharge plateau was 2.20 V (*vs.* Li/Li^+), offering a specific energy density of 1162 W h kg^{-1}. These initial results indicated that a battery composed of a graphene paper cathode and a lithium foil anode may have potential practical application as a power source. Nevertheless, the specific capacities of the papers in this study and the followings are not higher than the theoretical capacity of graphite, which diminishes their potential of practical application. Sun's research group designed specific experiments to explain the lower battery performances of the graphene papers.[95] For this purpose, three types of graphene

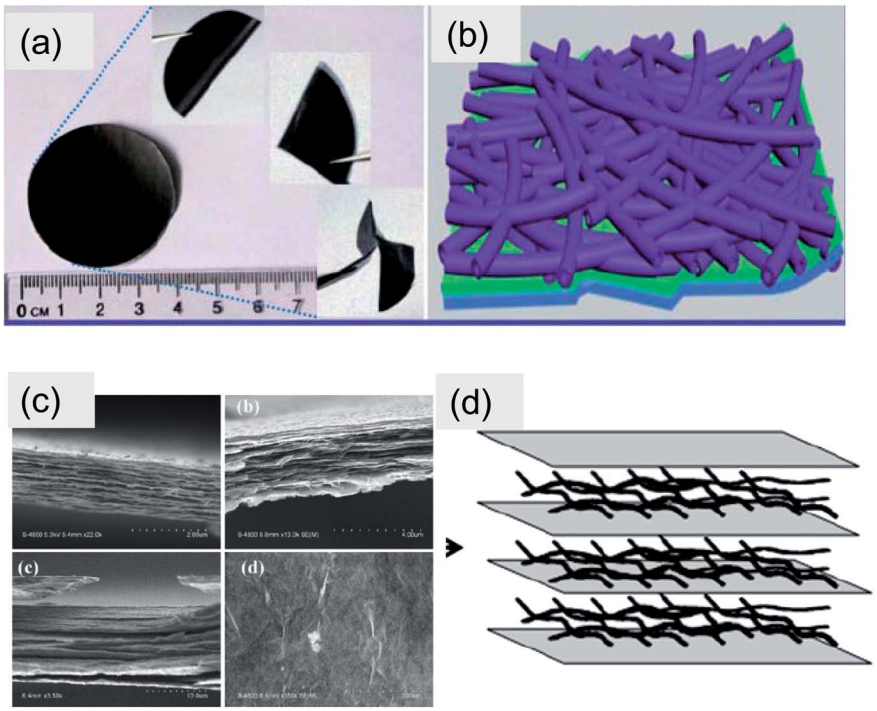

Fig. 12 Schematic diagrams and SEM images of the free-standing papers made from CNTs (a and b), graphene and their hybridization (c and d) (ref. 94–96).

papers, with thickness of ~1.5, 3 and 10 μm, respectively, were fabricated by vacuum-assisted filtration of reduced graphene nanosheets suspended in water. These papers delivered contrasting lithium storage capacities, with thinner papers consistently outperforming thicker ones. When cycled in a range of 0.01–3 V, the 1.5 μm paper gave rise to initial reversible specific capacities (the first 10 cycles) of ~200 mA h g^{-1} at a current density of 100 mA g^{-1}, while the 10 μm paper only presented ~80 mA h g^{-1} at a current density of 50 mA g^{-1}. After 100 cycles, a specific capacity of ~180 mA h g^{-1} was retained for the 1.5 μm paper; in contrast, only ~65 mA h g^{-1} remained for the 10 μm paper. The capacity decline with the paper thickness was explained by the dense restacking of graphene nanosheets and a large aspect ratio of the paper. The effective Li^+ diffusion distance in graphene paper is mainly controlled by the thickness of the paper, and the diffusion proceeds mainly in in-plane direction, cross-plane diffusion is restrained. As such, the effective contact of graphene nanosheets with electrolyte is limited and the efficiency of carbon utilization is very low in the thick papers. To support this explanation and suggest a potential way to improve the storage capacity of the flexible anode, they prepared free-standing hybrid papers by the vacuum-assisted filtration of graphene nanosheets (GNS) and CNTs both suspended in water, an approach that is environmentally benign.[96] The CNTs are randomly dispersed between the GNS and hence, the hybrid papers exhibit high mechanical strength and flexibility even after being annealed at 800 °C. The hybrid paper exhibited initial reversible specific capacities of ~375 mA h g^{-1} at 100 mA g^{-1}. The capacities remain above 330 mA h g^{-1} after 100 cycles, which are about 100 mA h g^{-1} higher than those of the graphene paper with nearly the same mass. The improved capacities were attributed to the contribution of the CNTs, which prevent restacking of the GNS, increase cross-plane electric conductivity of the paper and simultaneously, store Li ions. The related results are shown in Fig. 12.

There are also some other studies aiming at improving the capacities of graphene based flexible anodes. Liu, *et al.*, reported a novel method to fabricate graphene paper with folded structured graphene sheets.[97] Graphene oxide (GO) dispersion in water was first transferred into a Petri dish and frozen at −50 °C. The GO aerogel was formed by freeze-drying of the ice solid under vacuum. The GO aerogel could be converted into a graphene aerogel by directly heating. Graphene paper was obtained by pressing the graphene aerogel at 10 MPa. The density of the pressed aerogel was about 3 mg cm^{-3}, and had an electronic conductivity of 18 S cm^{-1}. For LIB tests, a small piece of graphene paper was used exclusively as the working electrode. CR2025 coin cells were fabricated using lithium metal as the counter electrode, Celgard 2400 as the separator, and 1 M $LiPF_6$ in EC–DMC–DEC (1 : 1 : 1 vol%) as the electrolyte. Charge–discharge tests were performed in a potential range 0.01–3.5 V *vs.* Li/Li^+. At current densities of 200, 500, 1000, and 1500 mA g^{-1}, the corresponding reversible specific capacities of the as-prepared graphene paper can reach 557, 268, 169, and 141 mA h g^{-1} anode, respectively. After 100 cycles, the reversible capacity was still maintained at 568 mA h g^{-1} at 100 mA g^{-1}. Zhao, *et al.*, reported flexible holey graphene paper electrodes with enhanced rate capability.[98] To create porous graphene sheets, aqueous GO suspension was treated with concentrated

HNO_3. The resulting holey GO papers were obtained by vacuum filtration. The rHGO working electrodes were typically 0.2–0.3 mg cm^{-2} and ~5 μm thick. Electrochemical measurements were carried out on rHGO papers using two-electrode coin cells with Li metal as the counter electrode. A microporous glass-fiber membrane was used as a separator, and a Cu foil was employed to connect the rHGO papers to external leads. The electrolyte consisted of 1 M $LiPF_6$ in EC–DMC (1 : 1, v/v). Galvanostatic measurements were conducted at various current densities, typically in a voltage range 0.02–1.5 V *vs.* Li/Li^+. The maximum specific capacity of over 400 mA h g^{-1} anode and capacity retention of >30% at 5.4 C (1 C equals a theoretical capacity of 372 mA h g^{-1}) were observed in the paper with an optimal in-plane pore size of 20–70 nm.

II Hybrid anodes from assembly of carbon and high-capacity nanomaterials. The capacities of full-carbon based flexible anodes are limited due to the limited capacity of graphite, *i.e.*, 372 mA h g^{-1}, a typical structure of carbon that is suitable for use as anode materials. The existing studies only conceptually provide some systems that show increased capacities. These systems are too brittle to be practically used.[98] Hence, much more studies have focused on incorporating high-capacity materials into the flexible paper and for this, nanostructured Si, nanostructured Sn, and nanostructured transition metal oxides were extensively investigated.[101–114] Yue, *et al.*, fabricated a nano-Si/MWCNTs free-standing paper electrode by a simple filtration and post sintering process.[101] The filtration method used sodium carboxymethyl cellulose (CMC) as a dispersing/binding agent. The nanosized Si particles were dispersed homogeneously and intertwined by the MWCNTs throughout the whole paper electrode. The cells were charged and discharged galvanostatically in a fixed potential window from 0.01 V to 1.5 V. After thermal sintering, the Si/MWCNTs paper electrode exhibited a significantly improved flexibility with a Si content of 35.6 wt% as compared with before sintering, and retained a specific capacity of 942 mA h g^{-1} after 30 cycles with a capacity fade of 0.46% per cycle. Cui's research group reported a novel anode structure by integrating a flexible, conductive CNTs network into a Si anode.[102] In the composite film, the infiltrated CNTs network functioned as both mechanical support and electrical conductor and Si as a high capacity anode material. Stainless steel mesh supported CNTs film, free-standing CNTs film, or free-standing CNTs–SiNP films were loaded into a chemical-vapor-deposition (CVD) tube furnace with silane as the silicon source. Such a free-standing film had a low sheet resistance of ~30 ohm per sq. To test the battery performance of the various free-standing films, pouch type half cells were made using free-standing films as the working electrode, a Celgard 2250 separator, and a Li metal foil as a counter electrode. The electrolyte was 1.0 M $LiPF_6$ in 1 : 1 w/w EC–DEC. The C–Si NW electrodes were cycled between 1 and 0.01 V. A film of 1 μm shows a high specific charge storage capacity (~2000 mA h g^{-1} Si) and a good cycling life.

Lee, *et al.*, fabricated Si NP–graphene paper composites in air.[103] Less than 30 nm Si nanoparticles were transferred from storage into a vial and exposed to air overnight to ensure formation of a surface layer of silicon oxide in order to facilitate dispersion in water. First, they were dispersed in a small amount of de-ionized water using sonication. Then, the GO suspension was added. The mixture was sonicated and then suction filtered. Composites of Si nanoparticles highly dispersed between graphene sheets, and supported by a 3D network of graphite formed by reconstituting regions of graphene stacks exhibited high Li ion storage capacities and cycling stability. The cells were cycled at a 100 mA g^{-1} constant current mode (2–0.02 V). The lithium storage capacities were >2200 mA h g^{-1} Si after 50 cycles and >1500 mA h g^{-1} Si after 200 cycles. Tao, *et al.*, reported self-supporting Si/RGO nanocomposite films prepared by thermal reduction of Si/graphene oxide nanocomposite, which was fabricated by dispersing silicon nanoparticles into an aqueous suspension of graphene oxide nanosheets.[104] The Si nanoparticles were well encapsulated in a RGO matrix and the Si/RGO composite had much higher reversible discharge capacity and a better cycle stability than pure nanosized Si particles and the RGO. The cells were charged and discharged galvanostatically in a fixed voltage window from 0.01 V to 1.5 V at 25 °C. The Si/RGO nanocomposite film delivered a reversible specific capacity of 1040 mA h g^{-1} in the first cycle, with an initial Coulombic efficiency of 63%. After 30 cycles, the capacity retention was 94% (about 977 mA h g^{-1}). Wang, *et al.*, reported 1D/2D hybridization for self-supported binder-free SiNWs–graphene paper based LIB anodes by a filtration method.[105] The SiNW–RGO electrode delivered a significantly high specific capacity of about 3350 mA h g^{-1} at 0.2 C (840 mA g^{-1}), which remained relatively constant over more than 20 cycles and exhibited a slow decay afterwards. The rate performance revealed that the galvanostatic charge–discharge profiles of SiNW–RGO were very similar at various rates from 0.1 C to 2 C. More importantly, under fast (2 C) and deep (2.0–0.002 V) discharge–charge cycling, a high specific capacity of *ca.* 1200 mA h g^{-1}, was obtained.

SnO_2 based flexible anodes are also receiving extensive research interest. Wang, *et al.*, developed a new facile route to fabricate N-doped graphene–SnO_2 sandwich papers.[106] A homogeneous graphene oxide suspension was prepared in H_2O/*N*,*N*-dimethylformamide (DMF) solvent by reduction with hydrazine monohydrate. A freshly prepared green 7,7,8,8-tetracyanoquinodimethane anion ($TCNQ^-$) acetonitrile solution was introduced to the above graphene suspension, after which a certain amount of $SnCl_2$ was quickly added to the solution. The obtained precipitate was washed and dried under vacuum. The paper-like samples were thermally treated to give final product. For testing, the working electrode was prepared by directly pressing a piece of sample paper onto a Cu mesh current collector. A Li metal foil was selected as the reference and counter electrode. The electrolyte was 1 M $LiClO_4$ in EC and DEC (1 : 1 in v/v). Galvanostatic discharge–charge measurements were performed over a potential range of 3–0.05 V *vs.* Li^+/Li. At the second discharge, the N-doped G-SnO_2 paper delivered a capacity of 918 mA h g^{-1} (the total weight of the N-doped G–SnO_2 paper was used to calculate the capacity values). More importantly, the N-doped G-SnO_2 papers exhibited high rate capacities. The specific capacity was maintained at values as high as 683 mA h g^{-1} and 619 mA h g^{-1} after the current density was increased to 1000 mA g^{-1} and 2000 mA g^{-1}, respectively.

Even at a current density of 5000 mA g^{-1}, the material still delivered a capacity of 504 mA h g^{-1}. Liang, *et al.*, reported a flexible free-standing graphene/SnO_2 nanocomposites paper (63 wt% SnO_2 and 37 wt% graphene) by coupling a simple filtration method and a thermal reduction together.[107] Compared with the pure SnO_2 nanoparticles (50–150 nm), the composite paper exhibited a better cycling stability. This is due to the graphene's high mechanical strength and elasticity which acts as a buffer minimizing the volume expansion and contraction of SnO_2 nanoparticles during the Li^+ insertion/extraction process. Charge–discharge measurements were carried out galvanostatically at a current density of 100 mA g^{-1} in a voltage range of 0.005–1.5 V. The specific capacity of the paper drastically increased during the initial 25 cycles as the wetting improved and then reached a high specific capacity of 526 mA h g^{-1} anode. After 50 cycles, the discharge capacity still remained 438.5 mA h g^{-1}, demonstrating about 83.4% retention of the reversible capacity of the 25th.

Lukman, *et al.*, reported free-standing SWCNTs/SnO_2 anode papers created *via* vacuum filtration of SWCNTs/SnO_2 hybrid material which was synthesized by the polyol method.[108] In a typical procedure, SWCNTs/SnO_2 hybrid material was dispersed into Triton X-100 surfactant. The suspension was then ultrasonically agitated. The as-prepared suspension was vacuum filtered. The resultant mat was then washed, dried, and then peeled off from the filter. To obtain highly crystalline SnO_2, the paper was heated at 300 °C. The CNTs form a 3D nanoporous network, in which ultra-fine SnO_2 nanoparticles, which had crystallite sizes of less than 5 nm, were distributed, predominately as groups of nanoparticles on the surfaces of SWCNTs bundles. For flexible cells, porous electrolyte film was prepared by the liquid–liquid extraction process containing P(VDF-HFP), NMP and nanoscale Al_2O_3 powders, and $LiPF_6$ solution in EC and DEC in a 1 : 2 ratio (v/v). The resulting electrolyte slurry was cast on the surface of the SWCNTs/SnO_2 anode paper and dried. It was then soaked in the 1 mol L^{-1} solution of $LiPF_6$/EC–DEC (volume 1 : 1) to make the porous polymer electrolyte. After the excrescent solution at the surface of the electrode was absorbed with filler paper, a flexible cell was fabricated from the SWCNTs/SnO_2 anode with the gel electrolyte, a lithium foil as a counter and reference electrode, and a porous polypropylene film as a separator, using an aluminum laminated pouch as the casing. To test the electrochemical performance, charge–discharge capacity measurements were carried out in a voltage range of 0.01–2 V at a constant current density of 25 mA g^{-1}. It was demonstrated that an anode paper with 34 wt% SnO_2 had excellent cyclic retention, with the high specific capacity of 454 mA h g^{-1} beyond 100 cycles. The SWCNTs/SnO_2 flexible electrodes can be bent to extremely small radii of curvature and still function well, despite a marginal decrease in the conductivity of the cell. The electrochemical response was maintained in the initial and further cycling process.

Besides the two highly desired materials, Si and Sn, some other nanostructured metal oxides were also investigated. Yang, *et al.*, reported graphene-coated Co_3O_4 fibers for high-performance LIBs.[109] To integrate graphene sheets and Co_3O_4 fibers into an assembly, the Co_3O_4 fibers were first modified by 3-aminopropyltrimethoxysilane (APS). The prepared GO suspensions were dispersed in water by a sonication process. Both the GO solution and the modified Co_3O_4 fibers were first mixed at pH 8. The GNS/Co_3O_4 composite papers were fabricated by filtering the above mixed solution through membrane filters followed by hydrazine reduction. For the testing of GNS/Co_3O_4 composite paper, the working electrode was prepared by directly pressing a piece of sample paper onto the Cu current collector. Electrochemical measurements were performed using Swagelok-type cells with lithium foil as the counter/reference electrode, Celgard 2400 membrane as the separator. The electrolyte was a 1 M $LiPF_6$ solution in a 1 : 1 (w/w) mixture of EC and DMC. Galvanostatic cycling test was performed in a voltage window of 0.01–3.00 V at a current density of 100 mA g^{-1}. The composite anodes exhibited reversible capacities of ~840 mA h g^{-1} after 40 cycles, excellent cyclic stability and good rate capacity. Wang, *et al.*, reported flexible free-standing hollow Fe_3O_4/graphene (H-Fe_3O_4/GS) films through vacuum filtration and thermal reduction processes, in which graphene formed a 3D conductive network, with hollow and porous Fe_3O_4 spindles captured and distributed homogeneously.[110] The electrochemical properties of the H-Fe_3O_4/GS composites as the negative electrode were characterized at room temperature. Li foil was used as the counter electrode. The electrolyte was 1 M $LiPF_6$ in a 1 : 1 w/w mixture of EC and DMC. Cyclic performances were performed in a voltage range 0–3.0 V. The H–Fe_3O_4/GS with 39.6 wt% graphene exhibited a high specific capacity (1555 mA h g^{-1} at 100 mA g^{-1} based on the total mass of the composites), enhanced rate capability and excellent cyclic stability (940 and 660 mA h g^{-1} at 200 and 500 mA g^{-1} after 50 cycles, respectively). Zhou, reported an Fe_2O_3/SWCNTs membrane with high Fe_2O_3 loading (88.0 wt%) prepared by oxidizing a flow-assembled Fe/SWCNTs membrane.[111] The Fe_2O_3/SWCNTs membrane shows a high reversible capacity of 1243 mA h g^{-1} at a current density of 50 mA g^{-1} and an excellent cyclic stability over 90 cycles at 500 mA g^{-1}.

Zhang, *et al.*, reported free-standing and bendable CNTs/TiO_2 nanofibres composite electrodes.[112] Chemically treated CNTs and TiO_2 nanofibres were dispersed evenly in distilled water and Triton X100 solution at a desired weight ratio followed by filtration. The free-standing films were cut to 10.0 mm × 10.0 mm pieces and assembled into CR2032 coin cells. The free-standing films weighed about 1 mg. In these cells, lithium foils acted as the counter electrode, and the electrolyte was 1 M $LiPF_6$ in EC–DMC (1 : 1 ratio). When tested in a range of 1.0–3.0 V *vs.* Li/Li^+ reference, the composite papers delivered about 35 and 25 mA h g^{-1} at 835 mA g^{-1} and 1670 mA g^{-1} rates, respectively at a CNTs/TiO_2 weight ratio of 1. Another type of freestanding graphene–TiO_2 paper was reported by Zhao, which is composed of mesoporous rutile TiO_2/C nanofibers with low carbon content (<15 wt%) prepared by electrospinning.[113] A large size (10 cm × 4 cm), flexible thin film is obtained after heat treatment under H_2–Ar. After optimization, the diameter of fibers can reach as small as ~110 nm, and the as-prepared rutile TiO_2 films show high initial electrochemical activity with the first discharge capacity as high as 388 mA h g^{-1} in a range of 1.0 and 3.0 V at room temperature. Moreover, very stable reversible

capacities of ~122, 92, and 70 mA h g^{-1} were achieved respectively at 1, 5 and 10 C rates with negligible decay rate within 100 cycles.

Yun, *et al.*, reported free-standing heterogeneous hybrid papers based on mesoporous γ-MnO_2 particles and acid-treated SWCNTs for LIB anodes.[114] The a-SWCNTs and mesoporous γ-MnO_2 particles were dispersed separately in distilled water by ultrasound treatment. The two dispersions were mixed and were then vacuum filtered. The high surface area mesoporous γ-MnO_2 particles are well dispersed throughout the nanoporous a-SWCNTs networks. These anodes exhibit a high electrical conductivity of 2.5 × 10^2 S cm^{-1} with high flexibility. The electrochemical performances of the composite papers were evaluated in a CR2016-type coin cell, employing a composite electrode with metallic lithium foil and 1 M $LiPF_6$ dissolved in a solution of EC–DMC–DEC (1 : 2 : 1, v/v) as the electrolyte. The cells were galvanostatically cycled between 0.01 and 3.0 V *vs.* Li/Li^+ at various current densities. For 50 wt% mesoporous γ-MnO_2 particle-loaded anodes, a high reversible capacity of 934 mA h g^{-1} anode was maintained after 150 cycles. Chen, *et al.*, reported "free-standing" ACNTs/PEDOT/PVDF membrane electrode,[88] which was lightweight, flexible, highly conductive, and mechanically robust. In a typical experiment, following production of the aligned CNTs on a quartz plate, a PEDOT film (100 nm) was deposited onto the CNTs array by chemical vapor phase polymerization. A thin film of ferric *p*-toluenesulfonate (Fe(III) tosylate) was coated on the aligned CNTs (ACNTs) array. The Fe(III) tosylate coated ACNTs array was then exposed to 3,4-ethylenedioxythiophene (EDOT) monomer vapor in the vapor-phase polymerization (VPP) chamber. Following air-drying, the PEDOT-coated ACNTs array was washed and dried. The ACNTs/PEDOT/PVDF membrane electrode had an electronic conductivity over 200 S cm^{-1}. The lithium-ion testing cell was assembled by stacking a porous polypropylene separator containing liquid electrolyte between the ACNTs/PEDOT/PVDF electrode and a lithium-foil counter electrode. The electrolyte was 1.0 M $LiPF_6$ in a 1 : 1 (v/v) mixture of EC and DMC. The capacity of the ACNTs/PEDOT/PVDF electrode was 50% higher than that observed for free-standing SWCNT paper. The cell was cycled at room temperature between 0 and 2.0 V at a constant current density of 0.1 mA cm^{-2} for the time required to reach the potential limit. The flexible electrode delivered a stable discharge capacity of 265 mA h g^{-1} after 50 cycles, which was significantly higher than the value obtained previously for SWCNT paper (173 mA h g^{-1}) under identical working conditions.

3. Electrolytes

For LIBs, the electrolyte is an electronic insulator working mainly as a medium that allows Li^+ to diffuse between anode and cathode. The selection of electrolyte can even determine the battery design, *e.g.*, when an optimal, flexible solid state electrolyte (SSE) is used. However, from the summaries of the flexible electrodes in the last part, it can be seen most of the existing studies used $LiPF_6$ based liquid electrolyte. This is a big safety concern because a large extent of mechanical deformation that is commonly exerted on flexible batteries is likely to induce internal short-circuit failures between electrodes, resulting in fire or explosion of the cells. As such, it is highly desirable to develop a flexible SSE for practical flexible LIBs applications.

For flexible LIBs, besides providing Li^+ diffusion channels and inhibiting electron transfer, a SSE can also work as a substrate that holds the electrode materials, functioning as a backing composite for the electrode. For such a configuration, the electrode materials slurries are usually pasted onto the SSE.[97] An optimal SSE must possess high ionic conductivity, good mechanical properties, no electrolyte leakage, low flammability, and low toxicity. In fact, most of the existing polymer electrolytes exhibit poor ionic conductivity, which is typically less than 10^{-4} S cm^{-1} in comparison to $LiPF_6$ based liquid electrolyte with a conductivity on the scale of 10^{-2} S cm^{-1}. Improving ion conductivity of SSE has been one of the key topics in polymer science and LIB research (including flexible LIBs). Many different strategies have been proposed, which can be found in several review papers.[115–134] One of the potential solutions is to explore low melting point ionic conductors such as plastic crystal electrolytes (PCEs), which are composed of lithium salts and plastic crystals bearing excellent solvating capability.[119,125,129–134] The ionic conductivity of such electrolytes can be in 10^{-3} S cm^{-1} scale. Nevertheless, they suffer deterioration of mechanical properties when delivering high ionic conductivity. To bring mechanical strength to the SSE, plastic crystal composite electrolytes (PCCEs) were developed, which use a polymer matrix as a mechanically reinforcing framework.[131–134] However, such an approach brings in another challenge, *i.e.*, an optimal composition ratio of the polymer matrix/PCE must be achieved to balance the mechanical properties and electrochemical performance. A large concentration of PCE in the PCCEs does deliver high ionic conductivity but reduce the mechanical properties; on the other hand, too much polymer addition will reduce the ionic conductivity of the SSE. It remains a big challenge to maintain high mechanical properties and ionic conductivity for the PCEs.

Some studies have advanced SSE research. The most recent studies on this topic were carried out by Lee's research group, who developed a facile approach to fabricate a highly bendable PCCE.[131] Fig. 13 presents a schematic diagram illustrating the UV-curing process and photographs depicting the physical appearance of solid state electrolytes PCE, X-PCCE, and S-PCCE. This is based on integration of a semi-interpenetrating polymer network (semi-IPN) matrix with a PCE and 1 M lithium bis-trifluoromethanesulfonimide (LiTFSI) in succinonitrile (SN). Both S-PCCE and X-PCCE provide excellent ionic conductivities of higher than 10^{-3} S cm^{-1} at room temperature. For evaluation of cell performance, the PCCE was fabricated directly onto a $LiCoO_2$ cathode/PVdF/Super-P in order to both impregnate the PCCE into the porous cathode and create a PCCE film onto the cathode. In this the PCCE serves both as an ion-conductive separator membrane and also as a solid electrolyte inside the cathode. A 2032 coin cell was assembled by sandwiching the PCCE-integrated cathode with a Li metal anode. The discharge capacities, discharge C-rate capability, and cyclability of the cells were estimated using a cycle tester. The discharge current

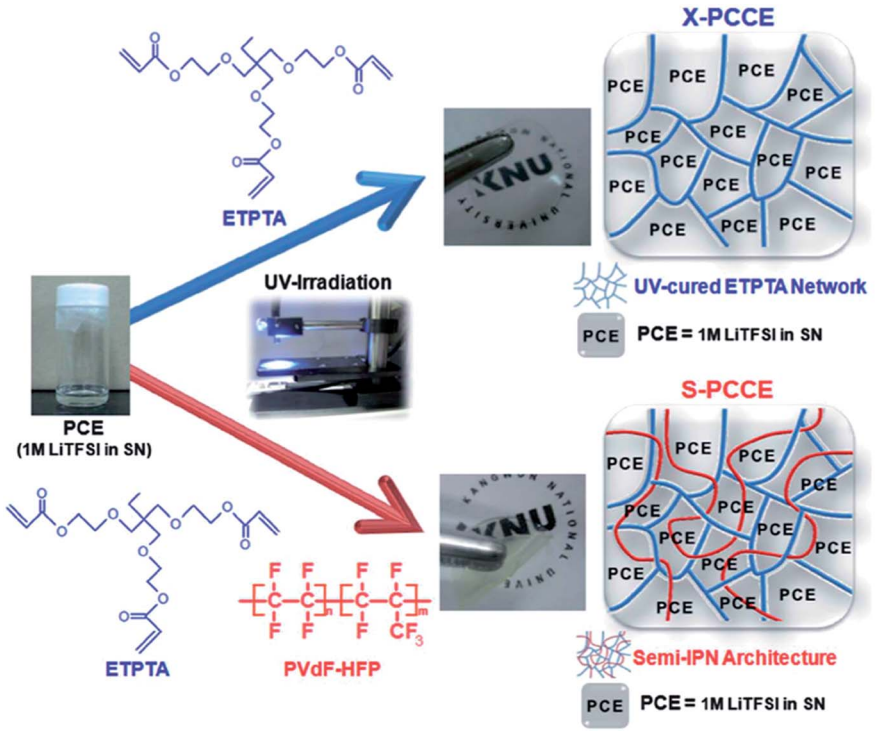

Fig. 13 A schematic diagram illustrating the UV-curing process and photographs depicting the physical appearance of solid state electrolytes. Reproduced from ref. 131 with permission. Copyright 2012 Royal Society of Chemistry.

densities were varied from 0.1 C (=0.02 mA cm^{-2}) to 1.0 C at a constant charge current density of 0.1 C under a voltage range between 3.0 and 4.2 V. The initial discharge capacity (at a discharge current density of 0.1 C) of the integrated cathode was ~138 mA h g^{-1}. Furthermore, the same group invented new imprintable polymer electrolytes for flexible LIBs.[133] The material consisted of a UV-cured polymer matrix, high-boiling point liquid electrolyte, and Al_2O_3 nanoparticles. The ionic conductivity of the c-GPE was higher than 10^{-3} S cm^{-1} at room temperature, which improved with increasing temperature. Cycling performance of the cell ($LiCoO_2$ cathode/c-GPE/lithium metal anode) was examined using a flat c-GPE film, where the cell was cycled between 3.0 and 4.2 V at a rate of 0.5 C. The capacity remained at ~130 mA h g^{-1} over 50 cycles. The cycling performance of the cell (Si anode/c-GPE/Li metal) using inversely-replicated c-GPE as an electrolyte was conducted with cycling from 0.01 and 1.5 V at a rate of 0.5 C. The initial charge was found to be 2680 mA h g^{-1}, but declined gradually afterwards as a result of the volume change in Si during cycling.

Lin, *et al.*, reported a wider operating SSE consisting of polysiloxane, PVDF, and LiTFSI.[134] The SSE shows a relatively high decomposition temperature of 275 °C. With 30 wt% LiTFSI, the ionic conductivities were 7.9×10^{-5} S cm^{-1} at 25 °C and 8.7×10^{-4} S cm^{-1} at 80 °C, respectively. The electrolyte was tested up to 5.17 V at 25 °C and 5.05 V at 60 °C, which were higher than currently used liquid organic electrolytes. Batteries employing $LiFePO_4$ as a cathode, a lithium foil as an anode and the SPE thin film as an electrolyte were assembled. At 25 °C, the initial discharge capacity at 0.2 C (the theoretical specific capacity of $LiFePO_4$ is 174 mA h g^{-1}, *i.e.*, 1 C) was 144 mA h g^{-1} and 98% of the capacity was retained after 100 cycles; the discharge capacity was 115 mA h g^{-1} after 100 cycles at 1 C and there was no significant decay after 200 cycles. Furthermore, the battery reached the discharge capacity of 144 mA h g^{-1} at the 100th cycle at 60 °C and 1 C.

4. Fundamental understanding and simulation of flexible batteries

LIBs only have less than 30 years of history, and there are many fundamental problems which remain unsolved. More challenging problems also exist in the flexible LIB systems, and some of them are currently not experimentally explorable. Mathematical modeling and computer simulations have proven to be powerful tools for gaining some important information in electrochemical energy conversion and storage.[135–143] For flexible LIBs, the simulations, when combined with experimental data, have provided some satisfactory description of the battery system, and several conclusions regarding battery performance and rate limitations have been made. In 2000, in order to model lithium-ion polymer cells with higher active material loadings and with energy densities and specific energies close to those of liquid LIBs, Arora, *et al.*, compared computer simulations with experimental data for Bellcore PLION® cells.[141] The Bellcore plastic lithium-ion cells consisted of porous composite positive and negative electrodes and a plasticized electrolyte, which was composed of 1 M $LiPF_6$ in 2 : 1 v/v mixture of EC/DMC and silanized fumed silica-filled P(VDF-HFP) copolymer matrix. The

composite electrodes were a mixture of MCMB 2528 or $LiMn_2O_4$, polymer binder, nonaqueous electrolyte, and conductive filler additive. The current collectors were expanded metal mesh made of aluminum or copper. Cells with different electrode thickness, initial salt concentrations, and higher active material loadings were examined using the mathematical model to understand the transport processes in the plasticized polymer electrolyte system. Agreement between the simulations and experimental data were obtained by using the contact resistance at the current collector/electrode interface as an adjustable parameter for different cells, with values vary from 20 to 35 $\Omega\ cm^{-2}$ based on separator area. The contact resistance was assumed to originate at the mesh current collector interfaces. Reducing the salt diffusion coefficient by a factor of two or more at the higher discharge rates was necessary to obtain better agreement with the experimental data. Based on the experimental data and model predictions, the authors concluded that the solution-phase diffusion limitations are the major limiting factor during high-rate discharges.

Wang, *et al.*, did mesoscale modeling of a Li-ion polymer cell by constructing finite element models of a 3D, porous cathode and analyzed them with a COMSOL multiphysics package.[142] Four types of cathode active material particles, arranged in both regular and random arrays, were modeled. Experimental studies of a Li/PEO–$LiClO_4$/Li_{1+x} Mn_2O_4 (where $0 < x < 1$) cell were used to validate the simulation results. Two parameters, Li ion diffusivity into Li_{1+x} Mn_2O_4 particles, and contact resistance at the interface between cathode particles and the current collector, were obtained by curve-fitting discharge curves of regular array models simulation results with experimental results. The average size of the $Li_{1+x}Mn_2O_4$ particles is ~3.6 μm. Diffusivities of Li ions were found to be 4×10^{-13}, 6×10^{-13}, 1×10^{-12} and 5×10^{-12} $cm^2\ s^{-1}$ for the $Li_{1+x}Mn_2O_4$ particles sintered at 800, 600, 500, and 450 °C, respectively. Contact resistances were found to be 3.5 $\Omega\ cm^{-2}$ for the $Li_{1+x}Mn_2O_4$ particles prepared at 600 and 800 °C, and 10.5 $\Omega\ cm^{-2}$ for particles prepared at 450 and 500 °C. Regular arrays were shown to increase achievable capacity from 5 to 50% of the theoretical capacity, compared with random arrays, at C/10 for samples sintered at 500 °C. Smaller particle sizes of active material particles were also shown to be beneficial for high power density applications and for low diffusivity active materials.

Kim, *et al.*, reported a modeling approach for scaling-up a lithium-ion polymer battery (LIPB).[143] A LIPB consisting of a Li[NiCoMn]O_2 positive electrode, a graphite negative electrode and a plasticized electrolyte was modeled. A cell, which is composed of two parallel plate electrodes of the battery, was chosen because the actual battery consists of the same repeating units of positive and negative electrode plates, polymer electrolytes and separators. The 2D potential and current-density distribution on the electrodes of a LIPB were predicted as a function of the discharge time using the finite element method. By comparing the experimental discharge curves of 10 and 26 A h LIPBs with the modeling results at discharge rates ranging from 0.5 to 5 C, it was confirmed that the parameters tuned for the electrodes of a small-scale battery can be applied to the electrodes of a large-scale battery provided the materials and compositions of the electrodes as well as the manufacturing processes are the same. Moreover, based on the modeling results of the potential and current-density distributions, the heat generation rate as a function of the discharge time and position on the electrodes was calculated. The 2D temperature distributions from the experiment and model were in good agreement. This modeling methodology provides important guidance for scaling-up manufacturing of the LIPB and modification of the electrode configuration.

Koo, *et al.*, developed a flexible LIB consisting of a $LiCoO_2$ layer, a LiPON electrolyte film, and Li metal wrapped in a PDMS sheet to enhance the mechanical stability.[69] To interpret the correlation between substrate conditions and stress from molar volume change during 100 cycles of charge and discharge, finite element analysis (FEA) simulation was carried out. The calculation showed that the capacities of LIBs transferred onto the PDMS substrates can be increased due to the prompt release of stresses by the molar volume change, which directly relates to the all-inclusive charge transfer resistance of Li ions. In addition, the reduction of induced stresses due to the transfer onto the PDMS substrate occurs at *x*-axis (along the substrate) positions. The compressive stress due to molar volume change changes to tensile stress at a certain degree of bending deformation along with increasing bending force. It is expected that the point of the compressive to tensile transition may be the most stable state for flexible LIB operation. Therefore, it was concluded that LIBs on flexible substrates can have higher stability and hence higher performance than those on brittle substrates.

5. Perspective

Although research and development of flexible LIB is still nascent, significant progress has been made in recent years, particularly in new electrode material development and in the processes for electrode preparation and for full cell assembly. Now, many novel nanomaterials have been incorporated into the flexible electrodes, either as lithium storage composites or as backing composites enhancing electrode strength (*e.g.*, current collector or substrates), such as nanostructured carbon (CNTs, fibers, and graphene), silicon NPs and NWs, nanostructured tin, nanostructured metal oxides, and nanostructured cathode materials, *etc.*, greatly improving the performances of the flexible electrodes. The invention and introduction of the nanosized materials not only triggered the invention of novel processes for electrode preparation and full battery assembly, but also opens windows for adopting the conventional process technologies in this field showing potential for mass production, *e.g.*, painting and printing technologies. Nevertheless, much more work is required before the new kinds of materials and processes are used for practical LIB design and full flexible LIBs are achieved with optimal match among the core components, *i.e.*, nanostructured electrode materials, shape-conformable solid electrolytes, and soft current collectors. Future effort should be made toward improving the electrode materials yield, optimizing flexible electrode design, and developing advanced processes for flexible electrodes preparation and full cell design.

5.1 Electrode materials and flexible electrodes

It is a fact that most of the existing studies on flexible LIB electrodes have focused on nanomaterial assemblies involving nanostructured carbon, nanostructured silicon, nanostructured tin, nanostructured metal oxides, and nanostructured cathode materials, *etc.* Among these, nanostructured carbon is an indispensible component. The presence of carbon effectively improves the electrical conductivity of electrode (particularly cathodes); however, the mechanical strength of the carbon based composite electrode is not high enough for practical application, particularly when a flexible substrate is omitted. Hence, the existing studies on free-standing flexible electrode are still in laboratorial scale, and the efficiency does not strongly support scaling up to mass production (to be addressed in detail in next part). As such, future work on flexible electrodes should focus on the following three aspects:

(1) Improve the mechanical strength of the flexible electrodes. In the present studies, most of the flexible electrodes are usually punched into circles with diameters $\leq$1 cm and are tested in half cells (with lithium foil as a counter electrode). Metal foils are used as a current collector and backing substrate, resulting in reduced flexibility of the electrodes. In practical applications, a non-metal flexible substrate is indispensable in providing with extra mechanical strength to the free-standing electrode for which development of a suitable binder is also necessary.

(2) Increase the active material loading and hence the overall battery capacities. So far, little attention has been paid to this parameter when designing and studying flexible LIBs, but for practical application, this should be addressed because higher capacities are highly desired. In this aspect, although there is no criterion, a balance between the high mass loading and electrical conductivity of the electrode should be systematically investigated and established. At higher mass loading, not only are the gravimetric energy density and volumetric energy density of a full battery affected, but the process of electrode and full-cell preparation may also be modified to enhance the mechanical strength of the electrode.

(3) Improve the efficiency and reduce the cost of flexible electrodes preparation. The introduction of novel nanomaterials does bring some breakthroughs in flexible LIBs research and development; however, high cost and low efficiency of the nanomaterial production is one of the biggest challenges when commercializing the batteries.

5.2 Full battery design

A majority of the existing studies have focused on half-cell flexible batteries, *i.e.*, the batteries use lithium foil as a counter electrode. These are suitable model systems allowing for evaluation of flexible electrodes and the active materials. However, practical full batteries are much more complicated as they require integrating and packaging each battery component into a single device. Therefore, to obtain a workable full flexible battery, besides optimizing the three core composites, other battery composites and processes must also be optimized, such as packaging materials and strain management. These have not been addressed in most of the existing research.[16] For example, in present fully flexible battery research, the typical packaging material is an aluminum pouch, composed of multiple polymer films and an Al layer. Full flexibility is not achieved from such a material. As a result, continuous bending or folding may lead to some wrinkling on the surface of the packaging, causing problems such as restricted mechanical deformability, increased internal resistance, and consequently reduced safety, *etc.* Obviously, in order to avoid deteriorating the performance of flexible LIB, it is necessary to introduce suitable packaging materials that are mechanically flexible and stretchable to the same extent as the individual components. To address these issues, systematic study on the mechanical and electrochemical properties of fully flexible batteries should be one of the most important topics in future research, and more in-depth analysis combined with mechanical studies is necessary. It is also important to combine fully flexible LIBs with electronic devices and study the mechanical behavior of the integrated device.

Future full battery design should also focus on finding effective process technologies to reduce cost and increase production. The approaches in the existing studies have not met this criterion. A potential solution is to fabricate composite electrodes by adopting hybridization technologies including printing and painting, coating, and spraying, *etc.*

Finally, a universal measurement standard for the mechanical properties of deformable LIBs should be established. The existing studies evaluate the mechanical properties of flexible batteries by repeatedly bending the batteries to certain angles and compare the electrochemical performances with the flat batteries (with no bending). This standard should comprise of cell size, form factors, and types of deformation.

5.3 Potential processes for flexible electrodes preparation and full cell assembly

In the existing studies, the flexible electrodes are usually prepared through processes like vacuum assisted filtration, CVD, sputtering, blade casting, or even more complex nanofabrication.[45,71] These processes are feasible in lab-scale studies, but they are insufficient for scaling up to mass production. Thus, some high-efficiency processes should be brought into this field, among which, printing and painting technologies have some evident advantages. First, the electrodes can be constructed rapidly. Second, the printing process allows for the combination of different electrode materials for the battery systems in which both high energy density components and high power density components are able to be embedded. Third, the processes are cost effective and therefore are highly potential for scaling up. They have already been considered a viable technique for large-scale fabrication of electronic devices (circuits, photovoltaics, displays, *etc.*) on many different types of substrate.[144–151] In future applications, these processes have the potential to be integrated into the production of more complete active devices. Consequently, there is huge interest in developing a fully paintable energy storage technology.[152,153] Several research groups have reported using printing and painting technologies to prepare LIBs electrodes and even full

batteries.[154–162] To better demonstrate the technologies, here, we list several representative studies.

Zhao, *et al.*, developed a novel and facile route of ink-jet printing a thin film SnO_2 anode for rechargeable LIBs.[159] The nano-sized electrochemically active SnO_2 was prepared *via* sol–gel method. SnO_2 nanoparticles were dispersed in polymeric hyper dispersant CH10B in mixture solvent (distilled water–absolute ethanol–diethylene glycol–triethanolamine–iso-propylalcohol) followed by ball-milling. Finally, the stable suspension SnO_2 and the stable acetylene black suspension were mixed by the volume ratio 1 : 1 and followed by addition of water-soluble sodium of carboxymethyl cellulose (CMC) as a binder. The as-prepared SnO_2 ink was transferred into a cleaned black Canon BC-03 cartridge and then ink-jet printed onto a commercial Cu foil. Thin film electrode was employed in a 2016-type coin cell. In order to achieve enough capacity for subsequent electrochemical measurements, a thicker electrode was prepared by printing 10 layers of SnO_2. Constant current charge–discharge measurements were performed in a potential range of 0.05–1.2 V. A high initial discharge capacity of 812.7 mA h g^{-1} anode was obtained at a constant discharge current density of 33 μA cm^{-2} over a potential range of 0.05–1.2 V.

Park, *et al.*, evaluated the electrochemical performances of printed $LiCoO_2$ cathodes with PVDF-HFP gel electrolyte for lithium ion microbatteries.[160] $LiCoO_2$ powder with an average size of 5.34 μm was used as a cathode material. The pastes were prepared by mixing $LiCoO_2$ powder and Emphos PS-21A that contained a mixture of long-chain phosphate esters of ethoxylated C_8–C_{12} alcohols as a dispersant and various vehicle compositions. Surface modification of the $LiCoO_2$ powder was performed *via* pyrolysis of resorcinol. A thick film was screen printed onto a platinum current collector/SiO_2/Si wafer using a stainless 400-mesh screen. The Pt current collector with an area of 1 cm × 1 cm was deposited by DC magnetron sputtering at a thickness of 300 nm. In 2012, Singh reported full LIBs consisting $LiCoO_2$ and $Li_4Ti_5O_{12}$ by a paintable process.[161] The paints were prepared as followed: for positive current collector paint, a mixture of purified Hipco SWNTs and 20% w/w SP Carbon was dispersed in NMP; for the cathode paint, a 85 : 5 : 3 (by wt) mixture of $LiCoO_2$, SP carbon and UFG was dispersed in a 4% w/v PVDF binder solution in NMP to a total solid content of 60% w/v; for the polymer separator paint, a 27 : 9 : 4 (by wt) mixture of Kynarflex®-2801, PMMA and fumed SiO_2 was dispersed in a binary solvent mixture of acetone and DMF; for the anode paint, an 80 : 10 (by wt) mixture of $Li_4Ti_5O_{12}$ and UFG was dispersed in a 7% w/v PVDF binder solution in NMP to a total solid content of 67% and for the negative current collector paint, commercially available copper conductive paint was diluted with ethanol. Full LIB cells were fabricated by sequentially spraying the component paints on a desired surface using an airbrush. The paints can be sprayed through a set of masks made according to desired device geometry. Cu and Al metal tabs were attached to the negative and positive current collectors respectively. The finished cell was transferred to argon filled glove box and activated by soaking in an electrolyte consisting of 1 M $LiPF_6$ solution in 1 : 1 (v/v) mixture of EC and DMC. The battery assembly is shown in Fig. 14. The spray painted full cell ($LiCoO_2$/MGE/$Li_4Ti_5O_{12}$) was cycled at a rate of C/8 between 2.7 and 1.5 V, where C is the current required to fully charge or discharge a cell in 1 h. 9 fabricated cells were connected in parallel and they could store a total energy of ~0.65 W h, equivalent to 6 W h m^{-2}.

Most recently, Sun, *et al.*, reported 3D printing of an interdigitated Li-ion microbattery consisting of $Li_4Ti_5O_{12}$ (40 nm) and $LiFePO_4$ (<200 nm).[162] Highly concentrated $Li_4Ti_5O_{12}$ (57 wt% solids) and $LiFePO_4$ (60 wt% solids) inks were prepared by first dispersing the particles in ethylene glycol (EG) water solution. These suspensions were then ball milled followed by a two-step centrifugation process. The collected nanoparticles were re-dispersed with appropriate addition of glycerol and aqueous hydroxypropyl cellulose (HPC) solution, and aqueous hydroxyethyl cellulose (HEC) solution. The resultant homogenized $Li_4Ti_5O_{12}$ mixture was composed of 27 wt% glycerol, 20–30 wt% EG, 9 wt% HPC, 1 wt% HEC, and DI water; whereas the $LiFePO_4$ contained 20 wt% glycerol, 20–30 wt% EG, 8 wt% HPC, 2 wt% HEC, and DI water. Before printing, interdigitated gold current collector patterns were patterned on a glass substrate by a combination of lithographic patterning and e-beam deposition. The inks were printed using a 3-axis micropositioning stage. The $LiFePO_4$ and $Li_4Ti_5O_{12}$ inks were housed separately and attached by luer-lok to a borosilicate micronozzle. After printing, the structures are annealed at 600 °C in argon gas

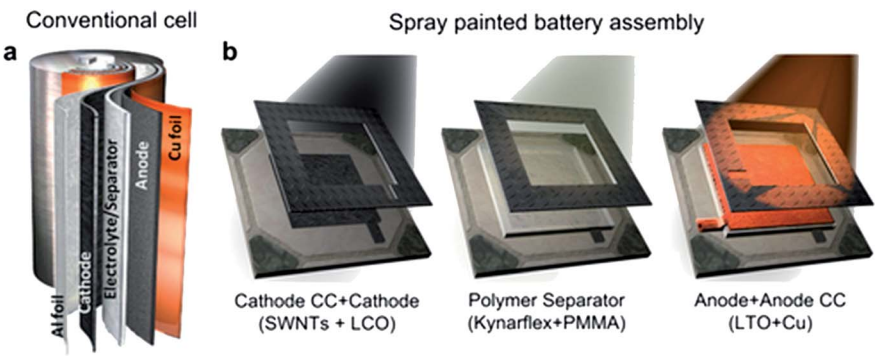

Fig. 14 A schematic diagram illustrating the process for making paintable batteries. Reproduced from ref. 161 with permission. Copyright 2012 Nature Publishing Group.

using a tube furnace. A thin-walled poly(methyl methacrylate) (PMMA) preform is laser cut and placed around the microbattery and sealed with PDMS gel, cured at 150 °C. The assembly was filled with liquid electrolyte and sealed with a small glass cover using additional PDMS. The 3D full microbattery (Fig. 15) was cycled between 1.0 and 2.5 V, and

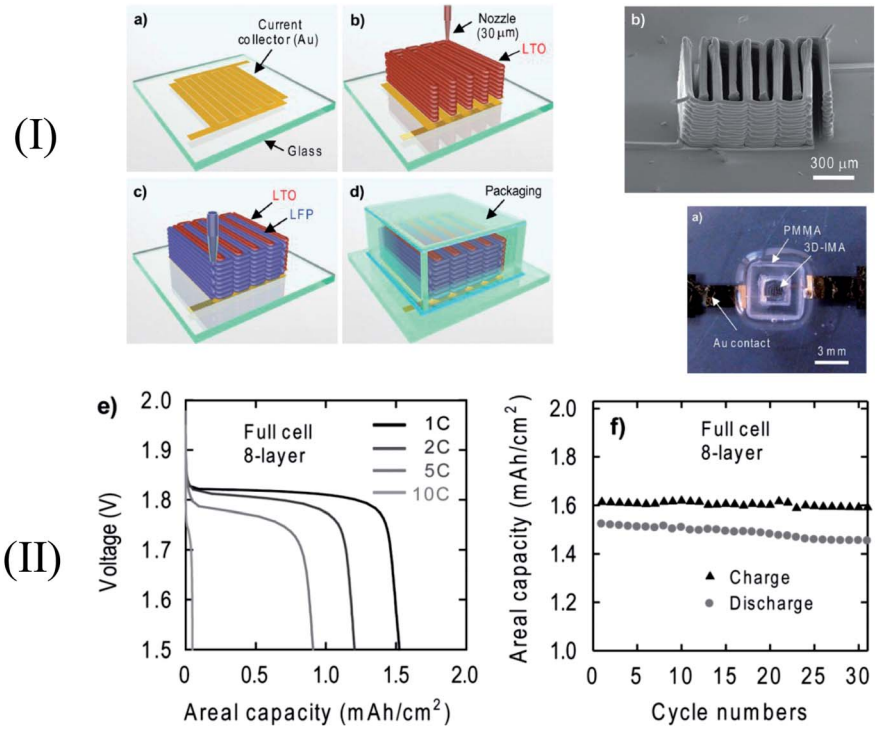

Fig. 15 (I) A schematic diagram illustrating 3D printing of interdigitated Li-ion microbattery architectures; and (II) performance of a full battery consisting of a $Li_4Ti_5O_{12}$ anode and a $LiFePO_4$ cathode tested between 1.0 and 2.5 V. Reproduced from ref. 162 with permission. Copyright 2013 WILEY-VCH Verlag GmbH & Co. KGaA, Weinheim.

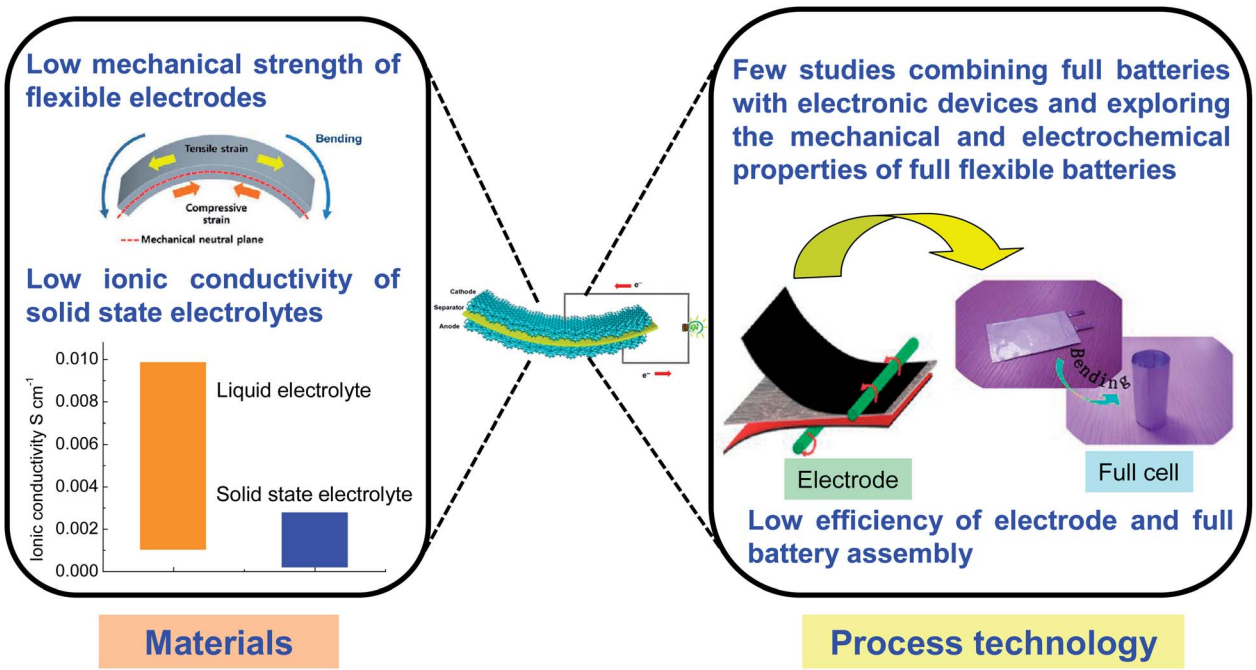

Fig. 16 An overview of the challenges in the materials and process technologies for future flexible lithium ion battery research. (The schematic diagrams used in this figure were copied from the ref. 56, 61, 62 and 69 cited in this review).

demonstrated a high areal energy density of 9.7 J cm^{-2} and a power density of 2.7 mW cm^{-2}.

Obviously, from these examples, it can be seen that the application of painting and printing technologies in LIBs fabrication is attractive and highly potential. However, one of the leading technical challenges is the preparation of suitable electrode ink.[159] Ball milling is a versatile process to enable homogeneous mix of the electrode components in the ink; however, the relatively lower yield of nanosized electrode materials might be a limiting factor, as mentioned in Section 5.1.

Finally, for being complete an overview of the challenges in the materials and process technologies for future flexible lithium ion battery research is summarized in Fig. 16.

6. Conclusion

Flexible lithium ion batteries have received rapidly increasing research interest in recent years, and much progress has been made in screening solid state electrolyte, soft current collectors, and electrode materials and in electrode design and full LIB cell design. Many novel nanomaterials have been incorporated into the flexible electrode, such as CNTs, carbon fibers, graphene, Si nanoparticles and nanowires, metal oxide nanoparticles and nanowires and cathode nanoparticles, *etc.*, greatly improving the battery performances of flexible electrodes. This review summarized the recent advances in flexible lithium ion battery research, with emphasis on the development of flexible electrodes and the processes for preparing the electrodes and full cell assembly. It is clear that many novel electrode and full-cell designs have high potential for practical application. Nevertheless, there are many big challenges for putting the new kinds of materials and processes in practical use and obtaining full flexible LIBs with optimized core components, *i.e.*, nanostructured electrode materials, shape-conformable solid electrolytes, and soft current collectors. Future opportunities for flexible lithium ion battery research includes the following several aspects: improvement of the electrode material production, enhancement of the mechanical strength of flexible electrode, improvement of the ionic conductivity and mechanical strength of solid state electrolytes, incorporating painting and printing technologies into battery assembly, and finally optimizing fully flexible battery design and systematically studying their mechanical and electrochemical properties, *etc.*

Acknowledgements

The authors are greatly grateful to Mr. Andrew Lushington, Mr. Craig Langford, and Mr. Stephen Lawes for taking time to read, discuss and edit this paper.

References

1 H. Nishide and K. Oyaizu, *Science*, 2008, **319**, 737–738.
2 A. Nathan, A. Ahnood, M. T. Cole, S. Lee, Y. Suzuki, P. Hiralal, F. Bonaccorso, T. Hasan, L. Garcia-Gancedo, A. Dyadyusha, S. Haque, P. Andrew, S. Hofmann, J. Moultrie, D. Chu, A. Flewitt, A. Ferrari, M. Kelly, J. Robertson, G. Amaratunga and W. Milne, *Proc. IEEE*, 2012, **100**, 1486–1517.
3 A. M. Biggar, *US Pat.* US3375136, 1968.
4 A. M. Gaikwad, A. M. Zamarayeva, J. Rousseau, H. Chu, I. Derin and D. A. Steingart, *Adv. Mater.*, 2012, **24**, 5071–5076.
5 A. M. Gaikwad, G. L. Whiting, D. A. Steingart and A. C. Arias, *Adv. Mater.*, 2011, **23**, 3251–3255.
6 Z. Q. Wang, Z. Q. Wu, N. Bramnik and S. Mitra, *Adv. Mater.*, 2014, **26**, 970–976.
7 T. Nagatomo, C. Ichikawa and O. Omoto, *J. Electrochem. Sci.*, 1987, **134**, 305–308.
8 Y. Gofer, H. Sarker, J. G. Killian, T. O. Poehler and P. C. Searson, *Appl. Phys. Lett.*, 1997, **71**, 1582–1584.
9 I. Sultanaa, M. Rahman, J. Wang, C. Wang, G. G. Wallace and H. K. Liu, *Electrochim. Acta*, 2012, **83**, 209–215.
10 J. C. Killian, B. M. Coffey, F. Gao, T. O. Poehler and P. C. Searson, *J. Electrochem. Soc.*, 1996, **143**, 936–942.
11 L. Nyholm, G. Nyström, A. Mihranyan and M. Strømme, *Adv. Mater.*, 2011, **23**, 3751–3769.
12 J. H. Shin, M. A. Henderson and S. Passerini, *J. Electrochem. Soc.*, 2005, **152**, A978–A983.
13 M. Mastragostino, F. Soavi and A. Zanelli, *J. Power Sources*, 1999, **81**, 729–733.
14 L. Sannier, R. Bouchet, S. Grugeon, E. Naudin, E. Vidal and J. M. Tarascon, *J. Power Sources*, 2005, **144**, 231–237.
15 A. Abouimrane, Y. Abu-Lebdeb, P. J. Alarco and A. Armand, *J. Electrochem. Soc.*, 2004, **151**, A1028–A1031.
16 H. Gwon, J. Hong, H. Kim, D. H. Seo, S. Jeon and K. Kang, *Energy Environ. Sci.*, 2014, **7**, 538–551.
17 S. Y. Lee, K. H. Choi, W. S. Choi, Y. H. Kwon, H. R. Jung, H. C. Shin and J. Y. Kim, *Energy Environ. Sci.*, 2013, **6**, 2414–2423.
18 G. Zhou, F. Li and H. H. Cheng, *Energy Environ. Sci.*, 2014, **7**, 1307–1338.
19 M. Armand and J. M. Tarascon, *Nature*, 2008, **451**, 652–657.
20 S. W. Lee, B. M. Gallant, H. R. Byon, P. T. Hammond and Y. Shao-Horn, *Energy Environ. Sci.*, 2011, **4**, 1972–1985.
21 S. W. Lee, B. M. Gallant, Y. M. Lee, N. Yoshida, D. Y. Kim, Y. Yamada, S. Noda, A. Yamada and Y. Shao-Horn, *Energy Environ. Sci.*, 2012, **5**, 5437–5444.
22 V. L. Pushparaj, M. M. Shaijumon, A. Kumar, S. Murugesan, L. Ci, R. Vajtai, R. J. Linhardt, O. Nalamasu and P. M. Ajayan, *Proc. Natl. Acad. Sci. U. S. A.*, 2007, **104**, 13574–13577.
23 F. Y. Su, C. H. You, Y. B. He, W. Lv, W. Cui, F. M. Jin, B. H. Li, Q. H. Yang and F. Y. Kang, *J. Mater. Chem.*, 2010, **20**, 9644–9650.
24 S. Flandrois and B. Simon, *Carbon*, 1999, **37**, 165–180.
25 Y. P. Wu, E. Rahm and R. Holze, *J. Power Sources*, 2003, **114**, 228–236.
26 J. Wang, R. Li and X. Sun, *Energy Environ. Sci.*, 2012, **5**, 5163–5185.
27 M. T. McDowell, S. W. Lee, N. Woo, D. William and Y. Cui, *Adv. Mater.*, 2013, **25**, 4966–4984.
28 J. R. Szczech and S. Jin, *Energy Environ. Sci.*, 2011, **4**, 56–72.

29 U. Kasavajjula, C. S. Wang and A. J. Appleby, *J. Power Sources*, 2013, **163**, 1003–1009.
30 W. J. Zhang, *J. Power Sources*, 2011, **196**, 13–24.
31 C. M. Park, J. H. Kim, H. Kim and H. Sohn, *Chem. Soc. Rev.*, 2010, **39**, 3115–3141.
32 J. Jiang, Y. Y. Li, J. P. Liu, X. T. Huang, C. Z. Yuan and X. W. Lou, *Adv. Mater.*, 2012, **24**, 5166–5180.
33 P. G. Bruce, B. Scrosati and J. M. Tarascon, *Angew. Chem., Int. Ed.*, 2008, **47**, 2930–2946.
34 K. T. Lee and J. Cho, *Nano Today*, 2011, **6**, 28–41.
35 H. Yang, X. L. Wu, M. H. Cao and Y. G. Guo, *J. Phys. Chem. C*, 2009, **113**, 3345–3351.
36 C. L. Liao and K. Z. Fung, *J. Power Sources*, 2004, **128**, 263–269.
37 Y. Jing and P. J. McGinn, *Electrochim. Acta*, 2013, **89**, 407–412.
38 P. P. Pronsini, R. Mancini, L. Petrucci, V. Contini and P. Villano, *Solid State Ionics*, 2001, **144**, 185–192.
39 H. Kim, R. C. Y. Auyeung and A. Pique, *J. Power Sources*, 2007, **165**, 413–419.
40 S. Ohta, S. Komagata, J. T. Seki, S. Morishita and T. Asaoka, *J. Power Sources*, 2013, **238**, 53–56.
41 S. Wagner and S. Bauer, *MRS Bull.*, 2012, **37**, 207–213.
42 C. Sealy, *Nano Energy*, 2013, **2**, 325–326.
43 J. Z. Wang, S. L. Chou, J. Chen, S. Chew, G. X. Wang, K. Konstantinov, S. Dou and H. K. Liu, *Electrochem. Commun.*, 2008, **10**, 1781–1784.
44 H. Gwon, H. S. Kim, K. U. Lee, D. Seo, Y. C. Park, Y. S. Lee, B. T. Ahn and K. Kang, *Energy Environ. Sci.*, 2011, **4**, 1277–1283.
45 Y. H. Kwon, S. W. Woo, H. R. Jung, H. K. Yu, K. Kim, B. H. Oh, S. Ahn, S. Y. Lee, S. W. Song, J. Cho, H. C. Shin and J. Y. Kim, *Adv. Mater.*, 2012, **24**, 5192–5197.
46 K. N. Han, H. M. Seo, J. K. Kim, Y. S. Kim, D. Y. Shin, B. H. Jung, H. S. Lim, S. W. Eom and S. I. Moon, *J. Power Sources*, 2001, **101**, 196–200.
47 A. M. Lackner, E. Sherman, P. O. Braatz and J. D. Margerum, *J. Power Sources*, 2002, **104**, 1–6.
48 A. Du Pasquier, T. Zheng, G. G. Amatucci and A. S. Gozdz, *J. Power Sources*, 2001, **97–8**, 758–761.
49 N. S. Choi and J. K. Park, *Electrochim. Acta*, 2001, **46**, 1453–1462.
50 A. Salzhauer, *Technol. Rev.*, 1998, **101**, 60–66.
51 Y. Liu, S. Gorgutsa, C. Santato and M. Skorobogatiy, *J. Electrochem. Soc.*, 2012, **159**, A349–A356.
52 B. A. Johnson and R. E. White, *J. Power Sources*, 1998, **70**, 48–54.
53 K. Wang, S. Luo, Y. Wu, X. F. He, F. Zhao, J. P. Wang, K. L. Jiang and S. Fan, *Adv. Funct. Mater.*, 2013, **23**, 846–853.
54 P. Arora, R. E. White and M. Doyle, *J. Electrochem. Soc.*, 1998, **145**, 3647–3667.
55 J. W. Braithwaite, A. Gonzales, G. Nagasubramanian, S. J. Lucero, D. E. Peebles, J. A. Ohlhausen and W. R. Cieslak, *J. Electrochem. Soc.*, 1999, **146**, 448–456.
56 L. B. Hu, H. Wu, F. La Mantia, Y. Yang and Y. Cui, *ACS Nano*, 2010, **4**, 5843–5848.
57 L. B. Hu, J. W. Choi, Y. Yang, S. Jeong, F. La Mantia, L. F. Cui and Y. Cui, *Proc. Natl. Acad. Sci. U. S. A.*, 2009, **106**, 21490–21494.
58 M. D. Lima, S. Fang, X. Lepró, C. Lewis, R. Ovalle-Robles, J. Carretero-González, E. Castillo-Martínez, M. E. Kozlov, J. Oh, N. Rawat, C. S. Haines, M. H. Haque, V. Aare, S. Stoughton, A. A. Zakhidov and R. H. Baughman, *Science*, 2011, **331**, 41–55.
59 X. L. Jia, C. Z. Yan, Z. Chen, R. R. Wang, Q. Zhang, L. Guo, F. Wei and Y. F. Lu, *Chem. Commun.*, 2011, **47**, 9669–9671.
60 A. K. Kercher, J. O. Kiggans and N. J. Dudney, *J. Electrochem. Soc.*, 2010, **157**, A1323–A1327.
61 N. Li, Z. P. Chen, W. C. Ren, F. Li and H. M. Cheng, *Proc. Natl. Acad. Sci. U. S. A.*, 2012, **109**, 17360–17365.
62 B. Liu, X. Wang, H. Chen, Z. Wang, D. Chen, Y. B. Cheng, C. W. Zhou and G. Z. Shen, *Sci. Rep.*, 2013, **3**, 1622–1628.
63 B. Liu, J. Zhang, X. F. Wang, G. Chen, D. Chen, C. W. Zhou and G. Z. Shen, *Nano Lett.*, 2012, **12**, 3005.
64 Y. P. Liu, K. Huang, Y. Fan, Q. Zhang, F. Sun, T. Gao, L. W. Yang and J. X. Zhong, *Electrochim. Acta*, 2013, **88**, 766–771.
65 S. Choi, J. I. Lee and S. Park, *J. Mater. Chem.*, 2012, **22**, 22366–22369.
66 K. Fu, O. Yildiz, H. Bhanushali, Y. Wang, K. Stano, L. Xue, X. Zhang and P. D. Bradford, *Adv. Mater.*, 2013, **25**, 5109–5114.
67 S. L. Chou, M. Ionescu, J. Z. Wang, B. Winton and H. K. Liu, *Nanosci. Nanotechnol.*, 2012, **4**, 169–172.
68 W. Ren, C. Wang, L. Lu, D. D. Li, C. W. Cheng and J. P. Liu, *J. Mater. Chem. A*, 2013, **43**, 13433–13438.
69 M. Koo, K. I. Park, S. H. Lee, M. Suh, D. Y. Jeon, J. W. Choi, K. Kang and K. J. Lee, *Nano Lett.*, 2012, **12**, 4810–4816.
70 A. Nojan, A. Mangilal, S. Sudhir and K. Varahramyan, *IEEE Trans. Nanotechnol.*, 2013, **12**, 408–412.
71 S. Xu, Y. H. Zhang, J. Cho, J. Lee, X. Huang, L. Jia, J. A. Fan, Y. W. Su, J. Su, H. G. Zhang, H. Cheng, B. W. Lu, C. J. Yu, C. Chuang, T. Kim, T. Song, K. Shigeta, S. Kang, C. Dagdeiren and I. Petrov, *Nat. Commun.*, 2013, **4**, 1543.
72 Q. Cheng, Z. M. Song, T. Ma, B. B. Smith, R. Tang, H. Yu, H. Q. Jiang and C. K. Chan, *Nano Lett.*, 2013, **13**, 4969–4974.
73 J. Wang, L. L. Li, C. L. Wong and S. Madhavi, *Nanotechnology*, 2012, **23**, 495401.
74 J. Y. Choi, D. J. Lee, Y. M. Lee, Y. G. Lee, K. M. Kim, J. K. Park and K. Y. Cho, *Adv. Funct. Mater.*, 2013, **23**, 2108–2114.
75 A. Vlad, A. A. Mohana Reddy, A. Ajayan, N. Singh, J. F. Gohy, S. Melinte and P. M. Ajayan, *Proc. Natl. Acad. Sci. U. S. A.*, 2012, **109**, 15168–15173.
76 J. H. Yun, G. B. Han, Y. M. Lee, Y. G. Lee, K. M. Kim, J. K. Park and K. Y. Cho, *Electrochem. Solid-State Lett.*, 2011, **14**, A116–A119.
77 H. Lee, Y. K. Yoo, J. H. Park, J. H. Kim, K. Kang and Y. S. Jung, *Adv. Energy Mater.*, 2012, **2**, 976–982.
78 Y. Yang, S. Jeong, L. B. Hu, H. Wu, S. W. Lee and Y. Cui, *Proc. Natl. Acad. Sci. U. S. A.*, 2011, **108**, 13013–13018.
79 M. S. Whittingham, *Chem. Rev.*, 2004, **104**, 4271–4301.
80 Y. G. Wang, W. R. Wang, E. Hosono, K. X. Wang and H. S. Zhou, *Angew. Chem., Int. Ed.*, 2008, **47**, 7461–7465.

81 L. Noerochim, J. Z. Wang, D. Wexler, M. Rahman, J. Chen and H. K. Liu, *J. Mater. Chem.*, 2012, **22**, 11159–11165.
82 Y. Q. Qian, A. Vu, W. Smyrl and A. Stein, *J. Electrochem. Soc.*, 2012, **159**, A1135–A1140.
83 Y. H. Ding, H. M. Ren, Y. Y. Huang, F. H. Chang and P. Zhang, *Mater. Res. Bull.*, 2012, **48**, 3713–3716.
84 C. Y. Wang, D. Li, C. O. Too and G. G. Wallace, *Chem. Mater.*, 2009, **21**, 2604–2606.
85 A. Abouimrane, O. C. Compton, K. Amine and S. T. Nguyen, *J. Phys. Chem. C*, 2010, **114**, 12800–12804.
86 S. S. Li, Y. H. Luo, W. Lv, W. Yu, S. Wu, P. X. Hou, Q. Yang, Q. Meng, C. Liu and H. M. Cheng, *Adv. Energy Mater.*, 2011, **1**, 486–490.
87 S. Y. Chew, S. H. Ng, J. Wang, P. Novak, F. Krumeich, S. L. Chou, J. Chen and H. K. Liu, *Carbon*, 2009, **47**, 2976–2983.
88 J. Chen, Y. Liu, A. I. Minett, L. Carol, J. Z. Wang and G. G. Wallace, *Chem. Mater.*, 2007, **19**, 3595–3597.
89 C. Zhong, J. Z. Wang, D. Wexler and H. K. Liu, *Carbon*, 2014, **66**, 637–645.
90 S. Q. Chen, W. Yeoh, Q. Liu and G. X. Wang, *Carbon*, 2012, **50**, 4557–4565.
91 H. R. Byon, B. M. Gallant, S. W. Lee and Y. Shao-Horn, *Adv. Funct. Mater.*, 2013, **23**, 1037–1045.
92 B. P. Vinyan, R. Nagar, V. Raman, N. Rajailakshmi, K. S. Dhathathreyan and S. Ramaprabhu, *J. Mater. Chem.*, 2012, **22**, 9949–9956.
93 B. J. Landi, M. J. Ganter, C. M. Schauerman, C. D. Cress and R. P. Raffaelle, *J. Phys. Chem. C*, 2008, **112**, 7509–7515.
94 X. Li, J. Yang, Y. Hu, J. Wang, Y. Li, M. Cai, R. Li and X. Sun, *J. Mater. Chem.*, 2012, **22**, 18847–18853.
95 Y. Hu, X. Li, D. Geng, M. Cai, R. Li and X. Sun, *Electrochim. Acta*, 2013, **91**, 227–233.
96 Y. Hu, X. Li, J. Wang, R. Li and X. Sun, *J. Power Sources*, 2013, **237**, 41–50.
97 F. Liu, S. Y. Song, D. F. Xue and H. J. Zhang, *Adv. Mater.*, 2012, **24**, 1089–1094.
98 X. Zhao, C. M. Hayner, M. C. Kung and H. H. Kung, *ACS Nano*, 2011, **5**, 8739–8749.
99 X. W. Yang, J. W. Zhu, L. Qiu and D. Li, *Adv. Mater.*, 2011, **23**, 2833–2838.
100 X. W. Yang, C. Cheng, Y. F. Wang, L. Qiu and D. Li, *Science*, 2013, **341**, 534–537.
101 L. Yue, H. X. Zhong and L. Z. Zhang, *Electrochim. Acta*, 2012, **76**, 326–332.
102 L. F. Cui, L. B. Hu, J. W. Choi and Y. Cui, *ACS Nano*, 2010, **4**, 3671–3678.
103 J. K. Lee, K. B. Smith, C. M. Hayner and H. H. Kung, *Chem. Commun.*, 2010, **46**, 2025–2027.
104 H. C. Tao, L. Z. Fan, Y. F. Mei and X. H. Qu, *Electrochem. Commun.*, 2011, **13**, 1332–1335.
105 B. Wang, X. L. Li, B. Luo, Y. Y. Jia and L. J. Zhi, *Nanoscale*, 2013, **5**, 1470–1474.
106 X. Wang, X. Q. Cao, L. Bourgeois, H. Guan, S. Chen, Y. Zhang, D. Tang, H. Li, T. Zhai, L. Li, Y. Bando and D. Golberg, *Adv. Funct. Mater.*, 2012, **22**, 2682–2690.
107 J. Liang, Y. Zhao, L. Guo and L. Li, *ACS Appl. Mater. Interfaces*, 2012, **4**, 5742–5748.
108 L. Noerochim, J. Z. Wang, S. L. Chou, D. Wexler and H. K. Liu, *Carbon*, 2012, **50**, 1289–1297.
109 X. L. Yang, K. C. Fan, Y. H. Zhu, J. H. Shen, X. Jiang, P. Zhao, S. Luan and C. Z. Li, *ACS Appl. Mater. Interfaces*, 2013, **5**, 997–1002.
110 R. H. Wang, C. H. Xu, J. Sun, L. Gao and C. C. Lin, *J. Mater. Chem. A*, 2013, **1**, 1794–1800.
111 G. M. Zhou, D. W. Wang, P. X. Hou, W. S. Li, N. Li, C. Liu, F. Li and H. M. Cheng, *J. Mater. Chem.*, 2012, **22**, 17942–17946.
112 P. Zhang, J. X. Qiu, Z. F. Zheng, G. Liu, M. Ling, W. Martens, H. Wang, H. J. Zhao and S. Q. Zhang, *Electrochim. Acta*, 2013, **104**, 41–47.
113 B. T. Zhao, R. Cai, S. M. Jiang, Y. J. Sha and Z. P. Shao, *Electrochim. Acta*, 2012, **85**, 636–643.
114 Y. S. Yun, J. M. Kim, H. H. Park, J. Lee, Y. Huh and H. J. Jin, *J. Power Sources*, 2013, **244**, 747–754.
115 R. Kokabang, I. I. Olsen and D. Shackle, *Solid State Ionics*, 1994, **69**, 320–335.
116 D. Fauteus, A. Massucco, M. Mclin, M. Vanburen and J. Shi, *Electrochim. Acta*, 1995, **40**, 2185–2190.
117 V. Chandrasekhar, *Adv. Polym. Sci.*, 1998, **135**, 139.
118 W. H. Meyer, *Adv. Mater.*, 1998, **10**, 439–448.
119 J. Y. Song, Y. Y. Wang and C. C. Wan, *J. Power Sources*, 1999, **77**, 183–197.
120 K. Murata, S. Izuchi and Y. Yoshihita, *Electrochim. Acta*, 2000, **45**, 1501–1508.
121 P. V. Wright, *MRS Bull.*, 2002, **27**, 597–602.
122 F. B. Dias, L. Plomp and J. B. J. Veldhuis, *J. Power Sources*, 2000, **88**, 169–191.
123 M. M. E. Jacob, E. Hackett and E. P. Giannelis, *J. Mater. Chem.*, 2003, **13**, 1–5.
124 A. M. Stephan, *Eur. Polym. J.*, 2006, **42**, 21–42.
125 A. Stephan and K. S. Nahm, *Polymers*, 2006, **47**, 5954–5966.
126 V. Di Noto, S. Lavina, G. A. Giffin, E. Negro and B. Scrosati, *Electrochim. Acta*, 2011, **57**, 4–13.
127 K. Xu, *Chem. Rev.*, 2004, **104**, 4303–4418.
128 M. Patel and A. J. Bhattacharyya, *Electrochem. Commun.*, 2008, **10**, 1912–1915.
129 P. C. Howlett, F. Ponzio, J. Fang, T. Lin, L. Jin, N. Iranipour and J. Efthimiadis, *Phys. Chem. Chem. Phys.*, 2013, **15**, 13784–13789.
130 Y. Shekibi, T. Youssof, J. Huang and A. F. Hollenkamp, *Phys. Chem. Chem. Phys.*, 2013, **14**, 4597–4604.
131 H. J. Ha, E. H. Eun, Y. H. Kwon, J. Y. Kim, C. K. Lee and S. Y. Lee, *Energy Environ. Sci.*, 2012, **5**, 6491–6499.
132 L. Fan, Y. Hu, A. Bhattacharyya and J. Maier, *Adv. Funct. Mater.*, 2007, **17**, 2800–2807.
133 E. Kil, K. Choi, H. Ha, S. Xu, J. A. Rogers, M. R. Kim, K. Y. Cho and S. Y. Lee, *Adv. Mater.*, 2013, **25**, 1395–1400.
134 Y. Lin, J. Li, Y. Lai, C. Yuan, Y. Cheng and J. Liu, *RSC Adv.*, 2013, **3**, 10722–10730.
135 T. F. Fuller, M. Doyle and J. Newman, *J. Electrochem. Sci.*, 1994, **141**, 1–10.

136 X. C. Zhang, W. Shyy and A. M. Sastry, *J. Electrochem. Sci.*, 2007, **154**, A910–A916.
137 J. Park, J. H. Seo, G. Plett, W. Liu and A. M. Sastry, *Electrochem. Solid-State Lett.*, 2011, **14**, A14–A18.
138 R. Spornitz, *J. Power Sources*, 2003, **113**, 72–80.
139 V. Ramadesigan, P. W. C. Northrop, S. De, S. Santhanagopalan, R. D. Braatz and V. R. Subramanian, *J. Electrochem. Sci.*, 2012, **159**, R31–R45.
140 A. A. Franco, *RSC Adv.*, 2013, **3**, 13027–13058.
141 P. Arora, M. Doyle, A. S. Gozdz, R. E. White and J. Newman, *J. Power Sources*, 2000, **88**, 219–231.
142 C. W. Wang and A. M. Sastry, *J. Electrochem. Sci.*, 2007, **15**, A1035–A1047.
143 U. S. Kim, C. B. Shin and C. S. Kim, *J. Power Sources*, 2009, **189**, 841–846.
144 F. Torrisi, T. Hasan, W. Wu, Z. Sun, A. Lombardo, T. S. Kulmala, G. Hsieh, S. Jung, F. Bonaccorso, P. J. Paul, D. Chu and A. C. Ferrari, *ACS Nano*, 2012, **6**, 2992–3006.
145 F. C. Krebs, J. Fyenbo and M. Jorgensen, *J. Mater. Chem.*, 2010, **20**, 8994–9001.
146 M. M. Ling and Z. N. Bao, *Chem. Mater.*, 2004, **16**, 4824–4840.
147 G. Blanchet and J. Rogers, *J. Imag. Sci. Tech.*, 2003, **47**, 296–303.
148 P. F. Moonen, I. Yakimets and J. Huskens, *Adv. Mater.*, 2012, **24**, 5526–5541.
149 J. Perelaer, P. J. Smith, D. Mager, D. Soltman, S. K. Volkman, V. Subramanian, J. G. Korvink and U. S. Schubert, *J. Mater. Chem.*, 2010, **20**, 8446–8453.
150 A. Teichler, J. Perelaer and U. S. Schubert, *J. Mater. Chem. C*, 2013, **1**, 1910–1925.
151 A. P. Quist, E. Pavlovic and S. Oscarsson, *Anal. Bioanal. Chem.*, 2005, **381**, 591–600.
152 L. Grande, V. T. Chundi, D. Wei, C. Bower, P. Andrew and T. Ryhänen, *Particuology*, 2012, **10**, 1–8.
153 L. B. Hu, H. Wu and Y. Cui, *Appl. Phys. Lett.*, 2010, **96**, 183502–183503.
154 S. Ohta, S. Komagata, J. Seki, T. Saeki, S. Morishita and T. Asaoka, *J. Power Sources*, 2013, **238**, 53–56.
155 H. Kim, J. Proell and R. Kohler, *J. Laser Micro/Nanoeng.*, 2012, **7**, 320–325.
156 J. H. Lee, S. B. Wee, M. S. Kwon, H. Kim, J. Choi, M. S. Song, H. B. Park, H. Kim and U. Paik, *J. Power Sources*, 2011, **196**, 6449–6455.
157 H. Kim, R. C. Y. Auyeung and A. Pique, *J. Power Sources*, 2007, **165**, 413–421.
158 F. Xu, T. Wang, W. R. Li and Z. Y. Jiang, *Chem. Phys. Lett.*, 2003, **375**, 247–251.
159 Y. M. Zhao, Q. Zhou, L. Liu, J. Xu, M. M. Yan and Z. Y. Jiang, *Electrochim. Acta*, 2006, **51**, 2639–2645.
160 M. S. Park, S. H. Hyun, S. C. Nam and S. B. Cho, *Electrochim. Acta*, 2008, **53**, 5523–5527.
161 N. Singh, C. Galande, A. Miranda, A. Mathkar, W. Gao, A. L. M. Reddy, A. Vlad and P. M. Ajayan, *Sci. Rep.*, 2012, **2**, 481.
162 K. Sun, T. S. Wei, B. Y. Ahn, J. Y. Seo, S. J. Dillon and J. A. Lewis, *Adv. Mater.*, 2013, **25**, 4539–4543.